

Structural geometry and evolution of releasing and restraining bends: Insights from laser-scanned experimental models

Shankar Mitra and Debapriya Paul

ABSTRACT

Experimental modeling is used to study the geometry and evolution of structures and related secondary faults along releasing bends and offsets and restraining bends on strike-slip faults. The controls of the relative positions of adjacent strike-slip faults on the geometry of the structures and the difference in geometries between bends and offsets are investigated. A new method of laser scanning is used to map the geometry and evolution of the structures and related faults. The models show that oblique releasing bends connecting approaching faults result in spindle-shaped basins, whereas transverse bends result in more S-shaped or rhomboidal basins. Offsets result in the distribution of strain over a wider area and a larger number of faults compared with preexisting bends, which result in fewer well-defined basin-bounding faults. Secondary faults include R, R', and Y Riedel shears near the main strike-slip faults and oblique normal faults in the center of the basin. Fault patterns exhibit en echelon geometries with a progressive step down into the deepest parts of the basin. Symmetric, asymmetric, and double basins may form in any of the structural settings, depending on the slip distribution among faults on the basin margins. For restraining bends, oblique (45°) bends connecting approaching faults result in spindle-shaped uplifts, whereas transverse or oblique (135°) bends connecting overlapping faults result in more rhomboidal or rectangular uplifts. The fold trends are at increasingly higher angles with

AUTHORS

SHANKAR MITRA ~ *ConocoPhillips School of Geology and Geophysics, University of Oklahoma, Norman, Oklahoma 73019; smitra@ou.edu*

Shankar Mitra holds the Monnett Chair and Professorship in Energy Resources at the University of Oklahoma. He received his Ph.D. from the Johns Hopkins University in 1977.

DEBAPRIYA PAUL ~ *ConocoPhillips School of Geology and Geophysics, University of Oklahoma, Norman, Oklahoma 73019; debapriya.paul-1@ou.edu*

Debapriya Paul is a Ph.D. student at the University of Oklahoma. He received his B.Sc. degree from the University of Calcutta, his M.Sc. degree from IIT, and his M.S. degree from the University of Oklahoma.

ACKNOWLEDGEMENTS

We thank Sandro Serra, Hong bin Xiao, Rick Groshong, Al Lacazette, and Ron Nelson for their comments and suggestions, and Shamik Bose for help with the laser scanning. We also acknowledge Paradigm for the university license of GO-CAD.

The AAPG Editor thanks the following reviewers for their work on this paper: Richard H. Groshong, Alfred Lacazette, and Ronald A. Nelson.

Copyright ©2011. The American Association of Petroleum Geologists. All rights reserved.

Manuscript received April 12, 2010; provisional acceptance June 2, 2010; revised manuscript received August 2, 2010; final acceptance September 27, 2010.

DOI:10.1306/09271010060

the strike faults for transverse and oblique (135°) bends. Secondary faults include en echelon reverse faults, which typically form along the steep limbs of asymmetric uplifts, normal faults, which are transverse or oblique to the axis of the structure, and R, R', and Y Riedel shears near the main strike-slip faults. The aspect ratios of the basins and uplifts increase with increasing displacement on the strike-slip faults. The results of these models can be used to interpret the structural and fault geometries in surface and subsurface structures formed along strike-slip faults.

INTRODUCTION

Strike-slip faults are commonly characterized by bends or offsets, marked by faults or fault systems with an oblique or transverse orientation to their general trend (Figure 1). A basement strike-slip fault may change position along a bend (Figure 1A) or by an offset of two separate fault segments (Figure 1B). The bends may be oblique or transverse to the main fault. Depending on their orientation relative to the sense of strike slip, bends or offsets in strike-slip faults are referred to as releasing or restraining (Figure 1C, D). Releasing bends or offsets form where the sense of shear on a strike-slip fault results in a component of fault-parallel extension (Figure 1C), whereas restraining bends or offsets form where the shear results in a component of fault-parallel contraction (Figure 1D).

The types of secondary structures and their orientations relative to the main fault were first described by Crowell (1974) and used to explain pull-apart basins and oblique compressive structures mapped by various authors in California basins. Subsequently, these models have been applied to explain structures in a variety of basins, such as in the collection of articles compiled by Sylvester (1984), Biddle and Christie-Blick (1985), and Cunningham and Mann (2007).

Most studies of restraining and releasing bends are based on surface, seismic, or remote-sensed data. Because data from all of these sources are incomplete, the interpretations are commonly made based on simplified conceptual models of these struc-

tures. Knowledge of the geometry of folds and faults formed in these settings and their progressive evolution through time would be useful in interpreting these structures in areas of incomplete data. One source of information for the detailed information is scaled experimental models of these structures.

The only published examples of restraining bends are the sandbox models of McClay and Bonora (2001) that investigated the shapes and evolution of structures and faults along preexisting jogs modeled above sliding base plates. These authors recognized the importance of documenting the structural relief associated with strike-slip structures and attempted to do so by building pseudo-three-dimensional (3-D) models from spaced serial sections. Several experimental models of releasing bends have been published. These include the sandbox models of Dooley and McClay (1987), Rahe et al. (1998), Basile and Brun (1999), Wu et al. (2009), and the clay models of Atmaoui et al. (2006). The first four articles all used precut jogs in sliding plates to simulate strike slip, whereas Atmaoui et al. (2006) used both sliding plates and distributed shear in their experiments. Dooley and McClay (1997) and Wu et al. (2009) attempted to qualitatively explain the variation in structural relief resulting from the oblique deformation.

The preexisting experimental models all used sliding metal plates with bends along them to simulate strike-slip deformation. These experimental configurations do not model deformation associated with preexisting offsets in the basement strike-slip fault, which is expected to be quite different from that associated with bends. Furthermore, with the exception of Atmaoui et al. (2006), who investigated the role of distributed shear in the development and intersection of Riedel shears, they all modeled the basement as perfectly rigid with the transition from strike-slip to oblique deformation occurring along a single preexisting jog.

In this article, we present experimental clay models of both restraining and releasing bends with various geometries of fault bends and fault offsets. The fundamental difference between the experimental configuration used in these experiments with previous models is that the basement

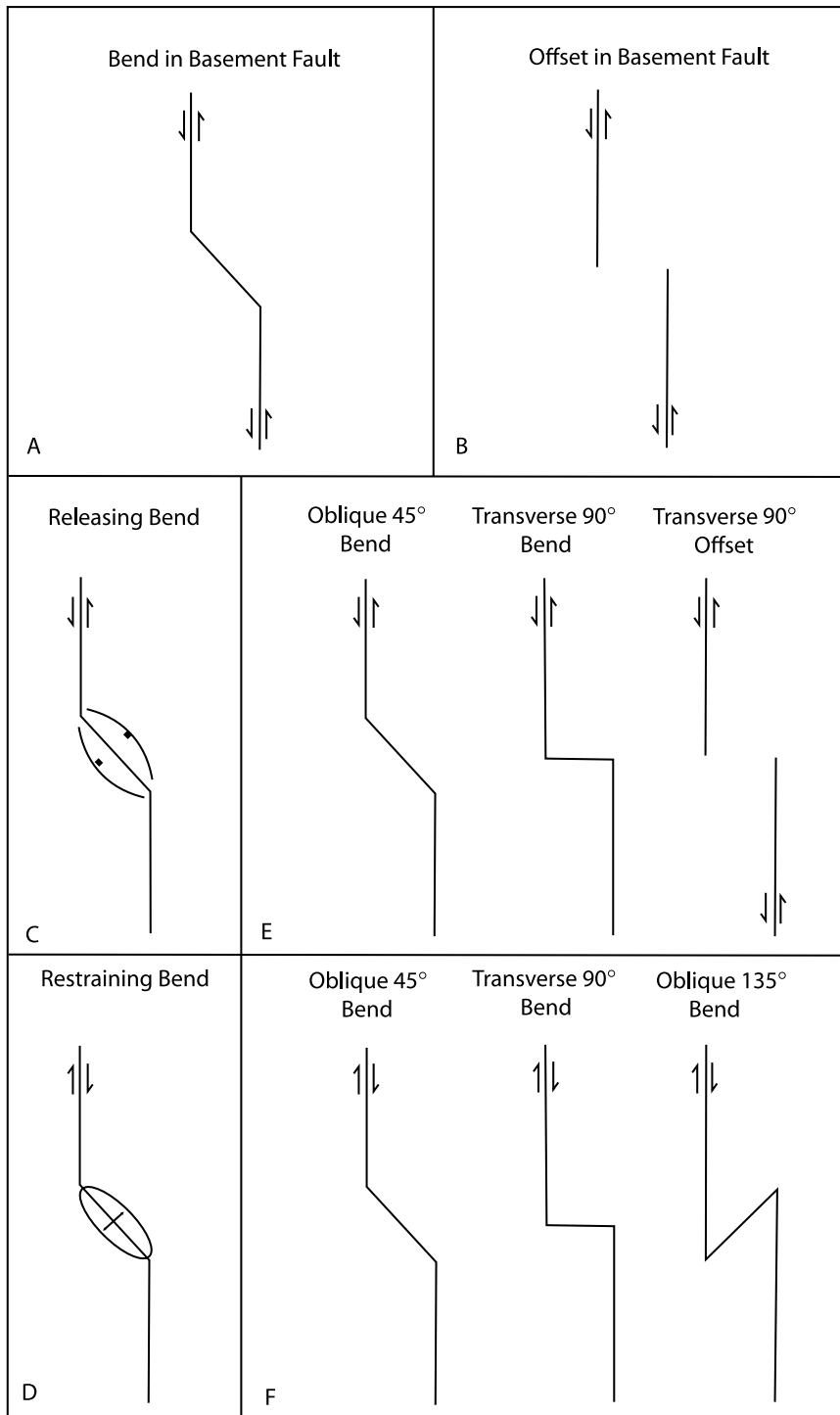
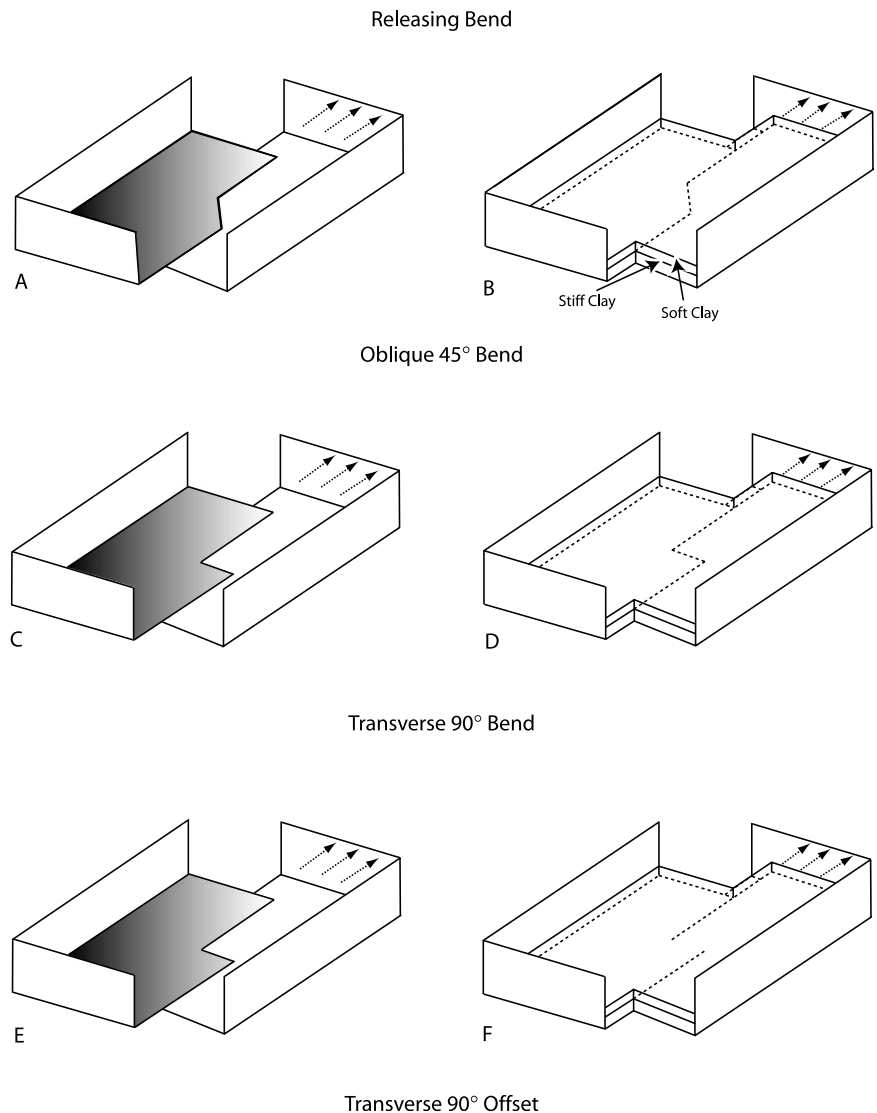


Figure 1. (A, B) Possible basement fault configurations for strike-slip faults. (A) Bend. (B) Offset. (C) Releasing bend. (D) Restraining bend. (E) Initial basement fault configurations used in experiments for releasing bends and offsets. (F) Initial basement fault configurations used in experiments for restraining bends. Figures 2 and 13 show details of the experimental setup for (E) and (F).

is modeled with stiff clay, which is significantly more rigid than the overlying soft clay representing the sedimentary cover, but which allows for a small component of deformation of the basement, especially in the immediate vicinity of the major faults. Sliding metal plates, which underlie the base-

ment, are used only to control the nature of deformation and the position of the bend or offset. Preexisting vertical cuts in the stiff clay define the initial geometry of the basement faults. This configuration also enables us to study the difference between releasing offsets and bends, which result

Figure 2. Experimental models conducted for releasing bends and offsets. (A, B) Oblique 45° bend in basement fault. (C, D) Transverse 90° bend in basement fault. (E, F) Transverse 90° offset in basement fault. For each experiment, the first figure shows the relationship between the underlying sliding plates, and the second figure shows the basement and sedimentary cover, and the preexisting fault cuts in the basement.



in very different geometries of structures and fault patterns in pull-apart basins (Figure 1). The specific experimental configurations depicted in this study are summarized in panels E and F of Figure 1 and described in more detail in the following sections.

The geometry and evolution of secondary faults for the top surface are studied in detail. In addition, using a new technique of laser scanning, we study the mutual relationships between structural relief and faulting with progressive deformation in contoured models for the surface. The renditions of the quantitative geometry of the deformed surfaces are directly comparable to structure contour maps of natural structures and, therefore, of most interest to petroleum geologists.

The results of the models are compared with natural examples of releasing and restraining bends to show how detailed interpretations of the structures can be improved through an understanding of the evolution of the structures.

RELEASING BENDS AND OFFSETS

Experimental Approach

Clay experiments are conducted to simulate the formation of releasing bends and offsets in strike-slip faults. The main advantage of using clay as the model material is that it allows a much better

definition of fault geometries and evolution and also enables the deformation to be studied for mature structures involving steep surfaces. The experimental setup consists of two overlapping metal plates, one of which is attached to a moving plate driven by motors, whereas the other is attached to a fixed plate. The lateral motion between the two base plates drives the strike-slip motion in the overlying stiff and soft clay, representing the basement and sedimentary layers (Figure 2). No shearing occurs along the contact between the stiff clay and the sliding plates. Basement is represented by stiff clay with a density of 1.85 g/cc and a thickness of 1 in. (2.5 cm). The overlying sedimentary layer is represented by soft water-based clay with a density of 1.6 to 1.65 g/cc and a thickness of 0.8 in. (2 cm). The density of the clay is adjusted by altering the water content of the clay, so that the clay has the appropriate consistency to deform by faulting without developing large cracks. No layering is used within the soft clay. The displacement rate for all experiments is 0.001 cm/s, corresponding to a strain rate of approximately 3×10^{-5} per second.

The experimental configurations used in this study differ from previous setups (Dooley and McClay, 1997; Rahe et al., 1998; Basile and Brun, 1999; Atmaoui et al., 2006; Wu et al., 2009) in that strike-slip motion is induced in both the stiff clay (basement) and the overlying soft clay (sedimentary cover) through sliding base plates at depth. Therefore, the sliding plates only control the nature of deformation and the location of the bend or offset. This approach enables us to study differences in deformation involving releasing bends and offsets in the strike-slip faults within the basement, whereas previous experiments modeled only releasing bends. Furthermore, using stiff clay to model basement instead of rigid plates, the basement deforms in the immediate vicinity of the faults to accommodate the deformation in these areas. In previous models, the top of the basement was represented by sliding plates, rendering the basement perfectly rigid in the vicinity of the faults.

Two experimental setups for the master faults in the basement are investigated: (1) bends, in which two parallel strike-slip faults are connected by an oblique (Figure 2A, B) or transverse (Figure 2C, D)

bend in the stiff clay representing the basement; and (2) offsets, in which two separate strike-slip fault segments in the basement are separated by a 90° offset in the stiff clay (Figure 2E, F). The initial configuration for the bend setup consists of two vertical cuts in the stiff clay connected by oblique or transverse bends, whereas the configuration for the offset setup consists of two parallel and offset vertical cuts. In both cases, the basement is underlain by two sliding plates that override each other to provide the strike-slip motion (Serra and Nelson, 1988). The bend configuration may represent an original geometry of the strike-slip fault (Crowell, 1974) or may result from two separate parallel segments that have connected along a transverse or oblique segment. The offset configuration more specifically addresses the linking of two adjacent strike-slip segments by the development of a transfer zone consisting of single or multiple oblique faults. These configurations result in significant differences in the geometry and faulting associated with the pull-apart basins. Two runs of each experiment are conducted to test for repeatability.

The progressive evolution of structures and secondary faults, and their orientations within a strike-slip system is mapped directly from photographs taken during various stages of the experiments. In addition, we use a new technique involving the analysis of the 3-D geometry of the top surface in the structures using laser scanning (see also Bose and Mitra, 2010). The technology of scanning surfaces by a laser scanner and developing a virtual 3-D model has been in use in numerous industries, particularly in 3-D animation. The same technology is applied here to gather 3-D information and thereby generate a virtual surface that can be used to visualize the development of the structure in much greater detail and to generate contour maps of surfaces. The scanning size is 13.5 × 10.1 in. (34.3 × 25.7 cm) with a resolution of 75 dots per inch (~0.015 in. point density). The scanner is placed face down, approximately 15 in. (38 cm) vertically above the clay cake, and top surfaces are scanned at approximately equal increments of deformation.

The sensor captures the laser beam that is projected on the surface, and the coordinates of the points are computed by the scanner using a triangulation

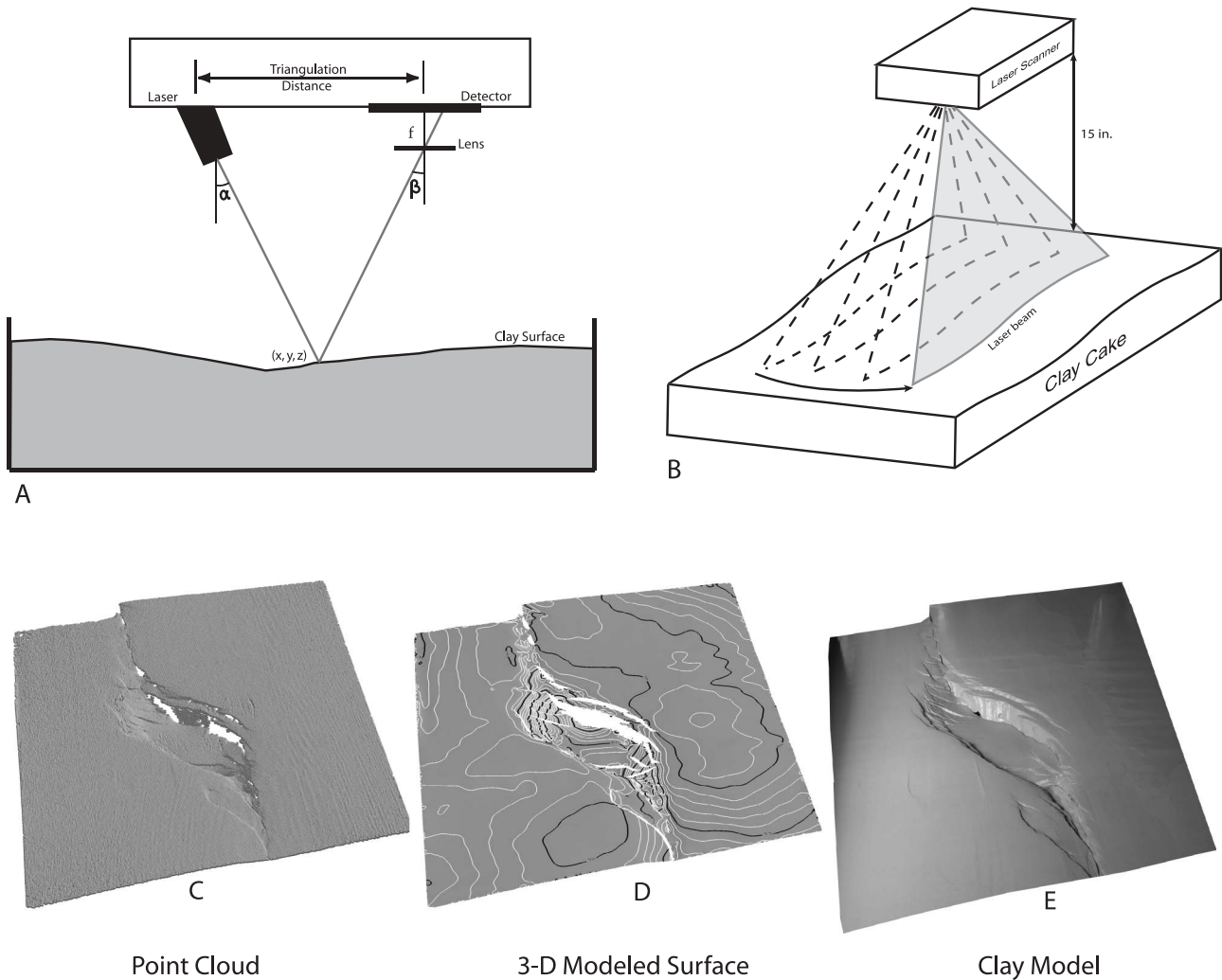


Figure 3. Laser scanning of experimental clay models. (A) Schematic diagram of the working principle of the laser scanner with the triangulation formed by the laser source, the detector, and the point on the clay surface from which the laser beam is reflected. (B) Schematic view of the laser scanner projecting a line and sweeping across the clay surface at a constant velocity (from Bose and Mitra, 2010; used with permission from AAPG). (C) Cloud of points obtained from the scanned surface and visualized in GO-CAD. (D) Modeled surface in GO-CAD cut by faults. (E) Oblique photograph of the top of the clay surface.

method (Figure 3A). The known parameters are the angle α at which the laser points out its beam on the surface, the angle β at which the sensor collects the laser beam (β is known if the focal length and the pixel size of the sensor are given) and the triangulation distance between the sensor and laser source (Petrov et al., 1998). Because all the geometric parameters are known, the coordinates x , y , and z on the surface are calculated using trigonometric methods. The laser source produces a line, and all data along that line are collected at the same time (Figure 3B). Moreover, twin arrays of four laser beams are used as source in this instrument for

cross-validating each data point by measuring it at least twice. The origin or reference coordinate system is determined automatically during each run by the first point scanned on the surface. It is therefore not necessary to move the scanner during the length of the experiment to spatially position the scanned surfaces in the same reference coordinate system.

The scanned data are exported as point files into the 3-D modeling software GoCAD (Bose and Mitra, 2010). The point clouds obtained (Figure 3C) are then used to build a surface. Fault polygons are built from visible breaks in the modeled surface (Figure 3D), and the geometries of the polygons

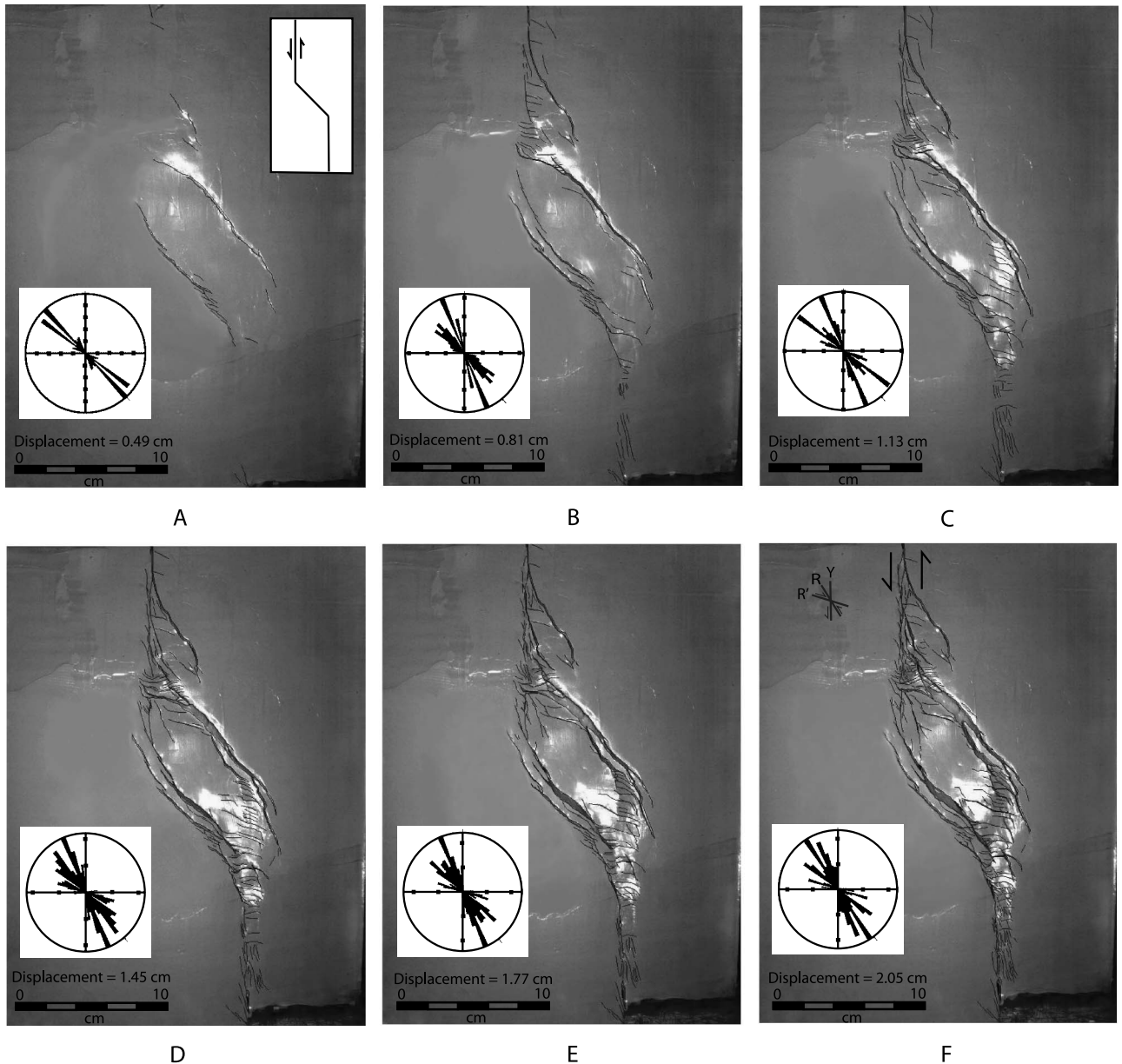


Figure 4. Clay models showing faults in the sedimentary cover for a releasing bend with an oblique (45°) bend connecting two strike-slip fault segments in the basement. The sense of slip on the strike-slip faults is left lateral. Insets in this and other figures for experimental models show initial fault cuts in the stiff clay. Panels (A–F) show the progressive evolution of the structure with increasing strike-slip displacement. Rose diagrams show the lengths of faults for different trends in 5° increments as a percentage of the total length of faults.

are checked against the traced fault cuts on photographs taken of the clay surface, which provide details of the fault geometry (Figure 3E). The modeled surface is cut by the fault polygons and contoured to depict their topology (Figure 3D). The contoured faulted surface provides an accurate quantitative rendition of the structural geometry, which can be compared directly with structure contour maps on natural structures.

Experimental Results

Oblique (45°) Bend

Initial movement on the base plate results in a broad depression oblique to the preexisting basement strike-slip faults in the area above the oblique bend (Figures 4A; 5A). This depression is bounded by two sets of faults dipping toward each other and trending approximately 42° to the basement

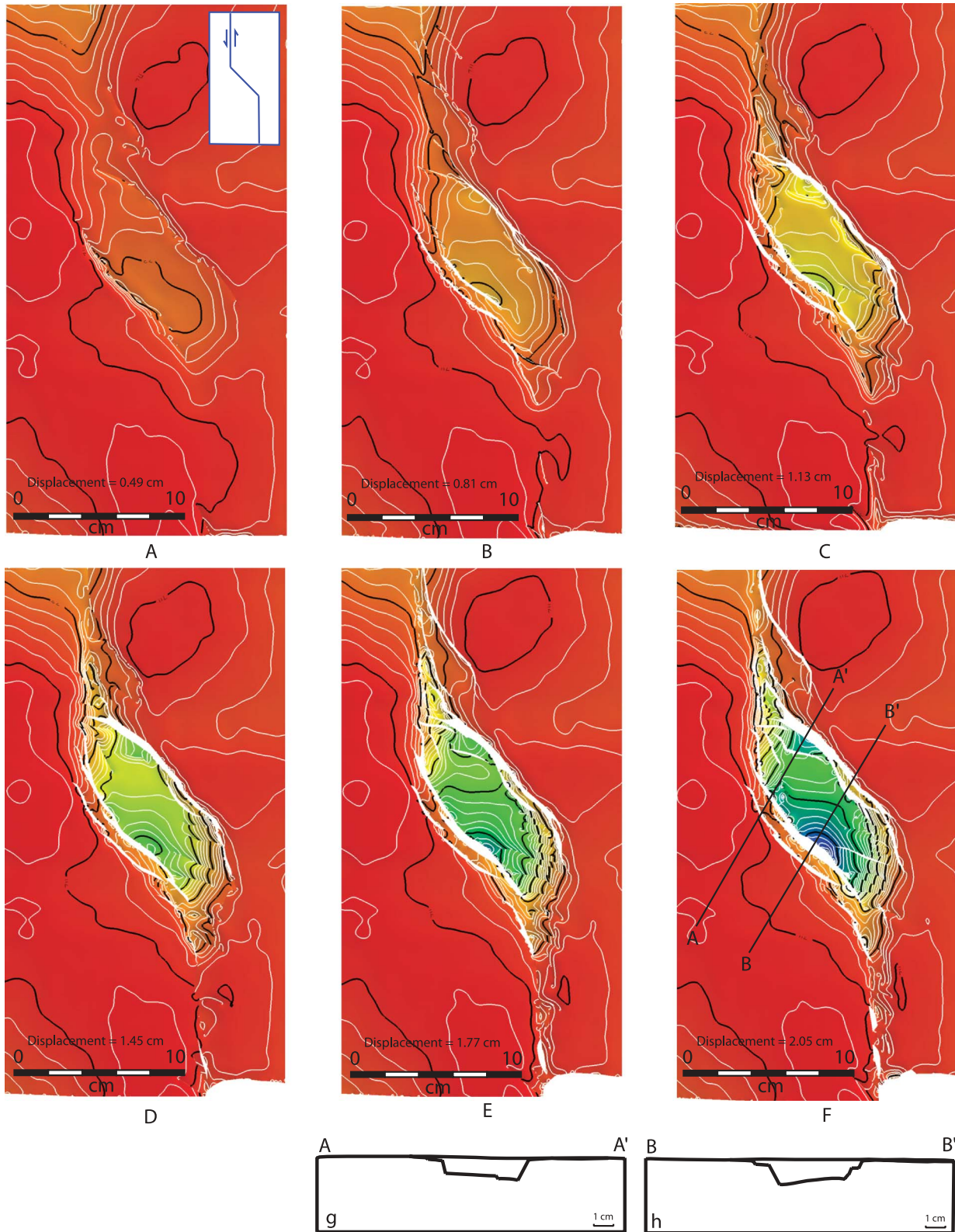


Figure 5. Three-dimensional geometry of the top of the sedimentary cover for a releasing bend with an oblique (45°) bend connecting two strike-slip fault segments in the basement. Panels A-F show the progressive evolution of the structure with increasing strike-slip displacement. Contours in this and subsequent diagrams are in intervals of 0.4 mm. Every fifth contour is shown in black. Color grids reflect structural elevation with red and yellow representing high areas and blue and green representing low areas. Note the formation of two diametrically opposite lows in the pull-apart basin. (G, H) Cross sections through top of clay showing final basin geometry and shift in polarity for cross sections AA' and BB'. Locations of the cross sections are shown in (F).

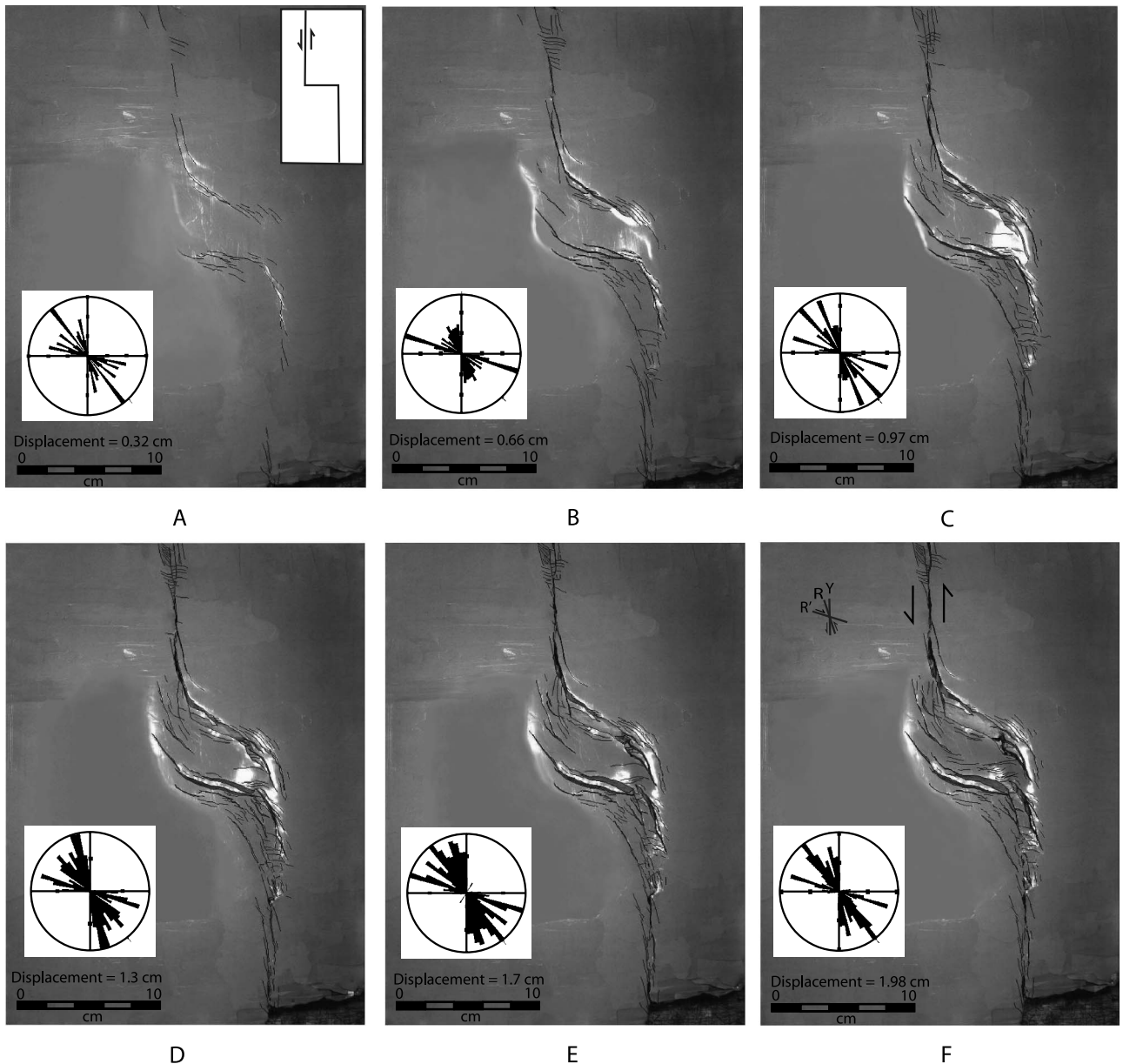


Figure 6. Clay models showing faults in the sedimentary cover for a releasing bend with a transverse (90°) bend connecting two strike-slip fault segments in the basement. Sense of slip on the strike-slip faults is left lateral. Panels A–F show the progressive evolution of the structure with increasing strike-slip displacement. Rose diagrams show the lengths of faults for different trends in 5° increments as a percentage of the total length of faults.

strike-slip faults that define the boundaries of the pull-apart basin. The angular measurements cited previously and in all experiments on pull-apart basins are made in a counterclockwise direction from the strike-slip faults. The individual faults are made up of two or more right-stepping en echelon segments, some of which eventually interact to form longer faults. With progressive deformation, these faults systems are rotated slightly by shear.

Immediately above the main vertical strike-slip faults, short segments of steep faults of two main sets trending approximately 15° and 80° to the basement strike-slip faults develop (Figure 4B, C). These faults are interpreted to be the R and R' Riedel shears associated with strike-slip faulting described and experimentally modeled by Tchalenko (1970), Tchalenko and Ambraseys (1970), Wilcox et al. (1973), and Harding (1985).

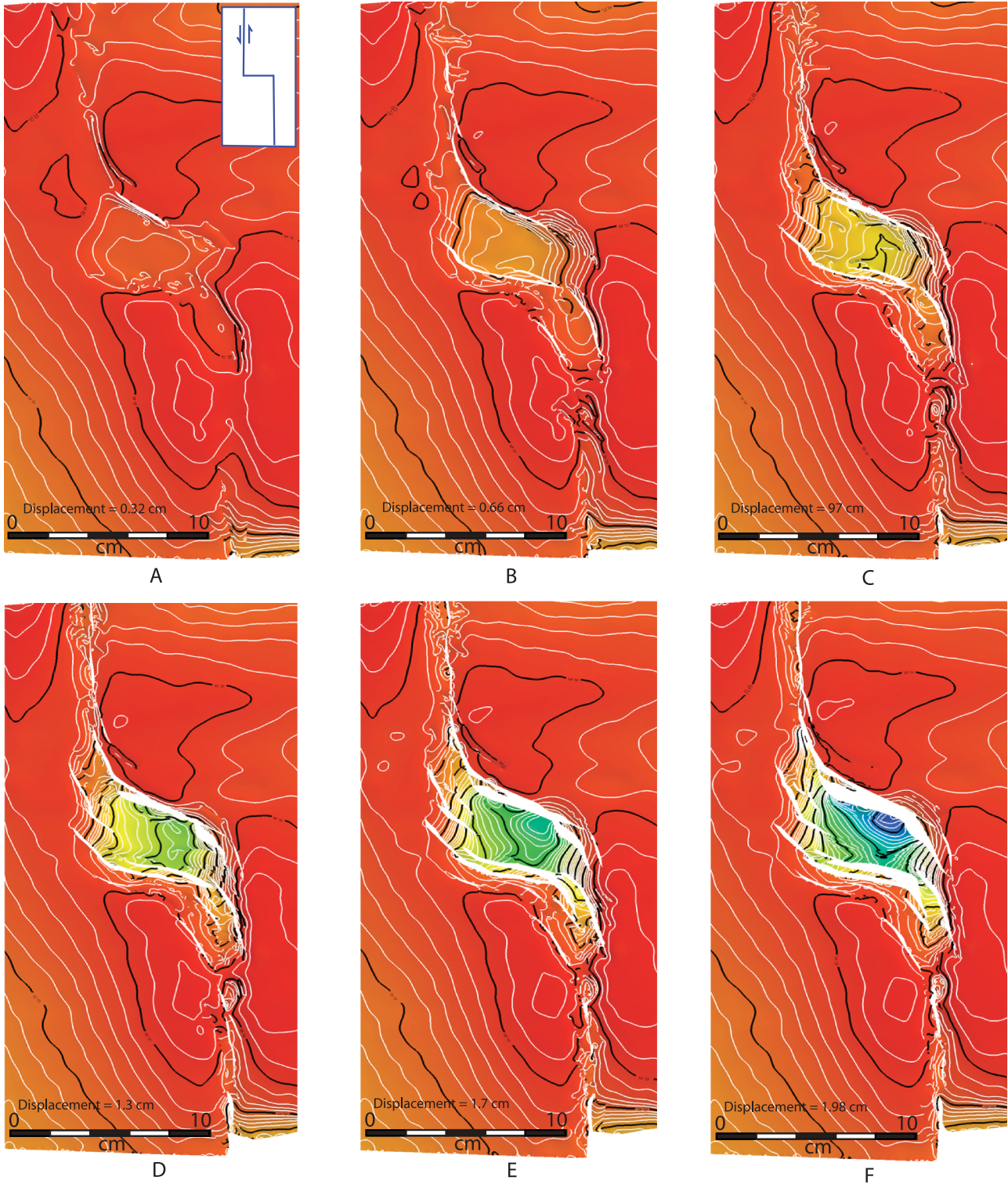


Figure 7. Three-dimensional geometry of the top of the sedimentary cover for a releasing bend with a transverse (90°) bend connecting two strike-slip fault segments in the basement. Panels A–F show the progressive evolution of the structure with increasing strike-slip displacement.

The normal faults in the central part of the basin curve into the orientations of the R shears in the vicinity of the basement strike-slip faults (Figures 4B, C; 5B, C). The resulting fault systems have a sigmoidal geometry. Rose diagrams of fault orientations show the progressive development of scatter because of the development of curved faults with varying components of normal and strike-slip motion (Figure 4A–C). Two major strike-slip faults develop at the surface directly above the preexisting cuts in the basement after about 0.8 cm of displacement.

Continuing deformation results in additional sets of major normal faults inward and approximately parallel to the original pair of fault systems. Additional fault systems with the same overall sigmoidal geometry form in other parts of the transfer zone and outside the central depression (Figures 4B–E, 5B–E). In the final stages of deformation, the longest pair of oblique faults connects with the two main systems of strike-slip faults, thus defining the boundary of the pull-apart basin (Figures 4F, 5F). The final rose diagram shows significant scatter of trends ranging from north to west because of the variation from strike-slip to normal fault trends, with a maximum density in an approximately northwest orientation (Figure 4F).

Examination of the contour patterns (Figure 5) suggests that the structural elevation steps down quite steeply across the normal faults bounding the pull-apart basin, but drops more gradually from the bounding system of strike-slip faults to the center of the basin. The central part consists of two separate depressions separated by a local high that develop during the late stages (Figure 5E, F). The axis connecting the centers of the two depressions is approximately parallel to the trend of the main strike-slip faults. Cross sections through the two depressions show a flip in polarity because of a change in fault displacement along trend within the basin (Figure 5G, H).

Transverse (90°) Bend

For a transverse bend (90°), the normal fault segments in the transfer zone form at a higher angle (58–78°) than in the case of the oblique jog (45°), and show left- and right-stepping patterns on op-

posite sides of the transfer zone (Figures 6A, B; 7A, B). Immediately above the basement strike-slip faults, R and R' Riedel shears develop as a series of en echelon faults, making angles of 15 and 82° to the main faults, respectively. The normal faults in the center of the pull-apart basin curve sharply clockwise toward the orientation of the R shears in the vicinity of the main strike-slip fault zones along the boundaries of the pull-apart basin (Figures 6C, D; 7C, D). With continuing shear, the major strike-slip faults break through to the surface as Y shears, defining the boundaries of pull-apart basin (Figures 6E, F; 7E, F). As in the case of the oblique-bend experiment, multiple sets of faults form in the pull-apart basin, especially close to the main strike-slip fault zone. The orientations of the faults show a wide variation in trends ranging from north–northwest to west–northwest, with the most dominant trend in the center of the basin being about northwest in the final stage (Figure 6F).

Because of the sharper bends and changes in the trends of the faults in the transfer zone, the pull-apart basin associated with a transverse bend has a more S-shaped or rhomboidal geometry than the spindle-shaped geometry in the case of an oblique bend. The contours show that the deepest part of the basin is located toward one of the major transfer faults, so that the pull-apart basin has a more asymmetric shape, with a sharper drop of contours on one side (Figure 7E, F). The sides of the basin are marked by a more gradual change in elevation with the structure contours cut by secondary faults. Different basin shapes may result depending upon the slip distribution among the different faults.

Transverse (90°) Offset

This setup has two cuts in the basement that eventually form the bounding strike-slip faults offset along a transfer zone. The main purpose of conducting this experiment was to understand the difference in the geometry of the pull-apart basin when no connecting bend exists in the basement fault. The faults in the transfer zone develop with ongoing strike-slip deformation, independent of a connected basement fault (Figures 8, 9). Our experiments show that a transverse offset results in the optimum configuration for the development of a

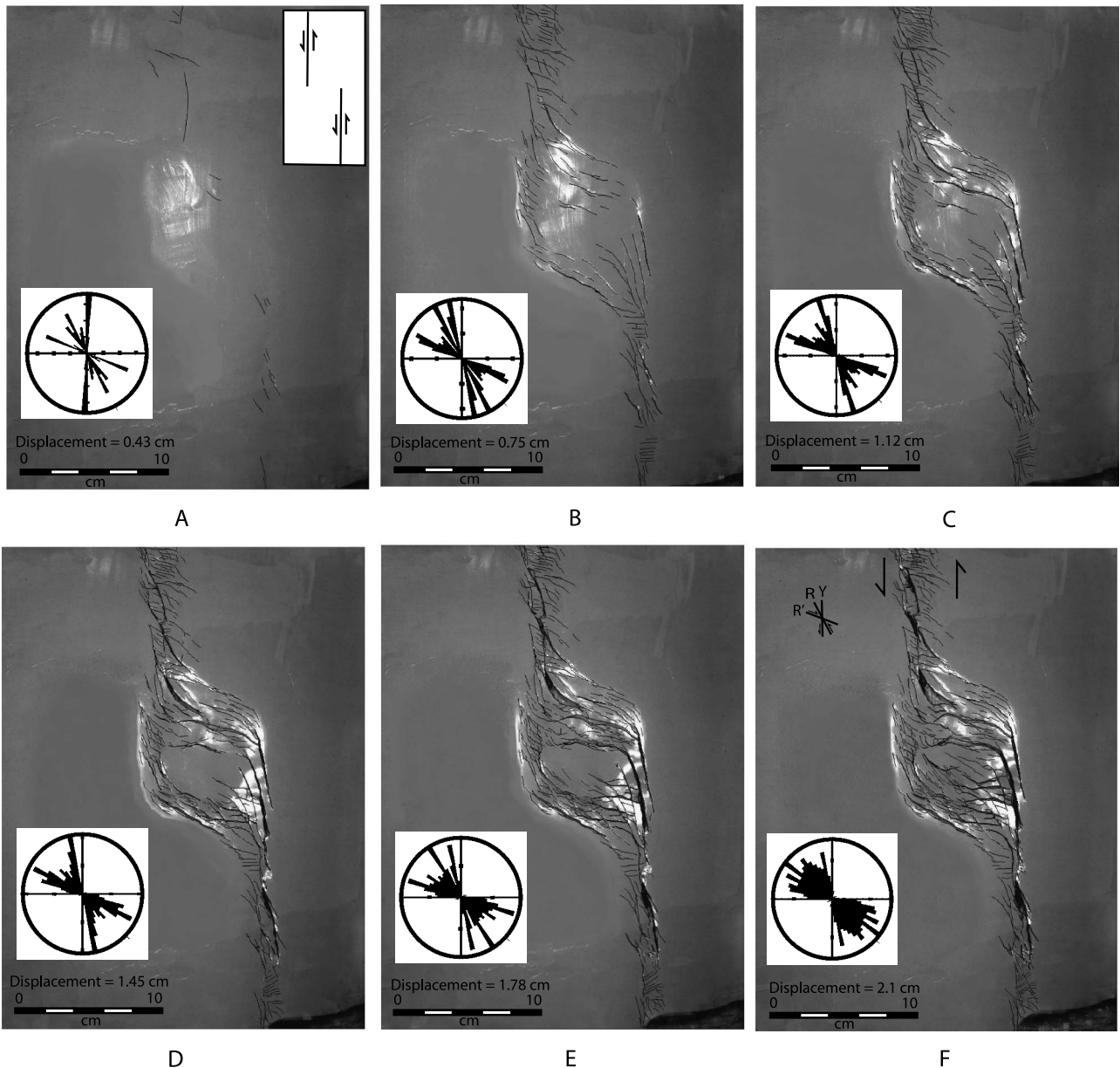


Figure 8. Clay models showing faults in the sedimentary cover for a releasing offset with a transverse (90°) offset between two strike-slip fault segments in the basement. The sense of slip on the strike-slip faults is left lateral. Panels A–F show the progressive evolution of the structure with increasing strike-slip displacement. Rose diagrams show the lengths of faults for different trends in 5° increments as a percentage of the total length of faults.

transfer zone of connecting faults. Experiments involving overlapping or approaching patterns do not result in well-defined pull-apart basins because they both involve a large transfer zone area. This suggests that for two approaching strike-slip fault segments, connecting faults in the transfer zone will most likely start to develop when the end points of the two strike-slip segments are directly opposite each other in a transverse offset position.

Initial deformation results in the formation of a large number of short en echelon normal faults in the area of the transfer zone (Figures 8A, B; 9A, B). The central parts of the faults trend at angles of 53° to 63° to the main strike-slip fault zone. At the same time, a series of en echelon R and R' Riedel shears form above the main basement faults, at angles of 18° and 70° with respect to the basement strike-slip faults, respectively. With increasing strike-slip

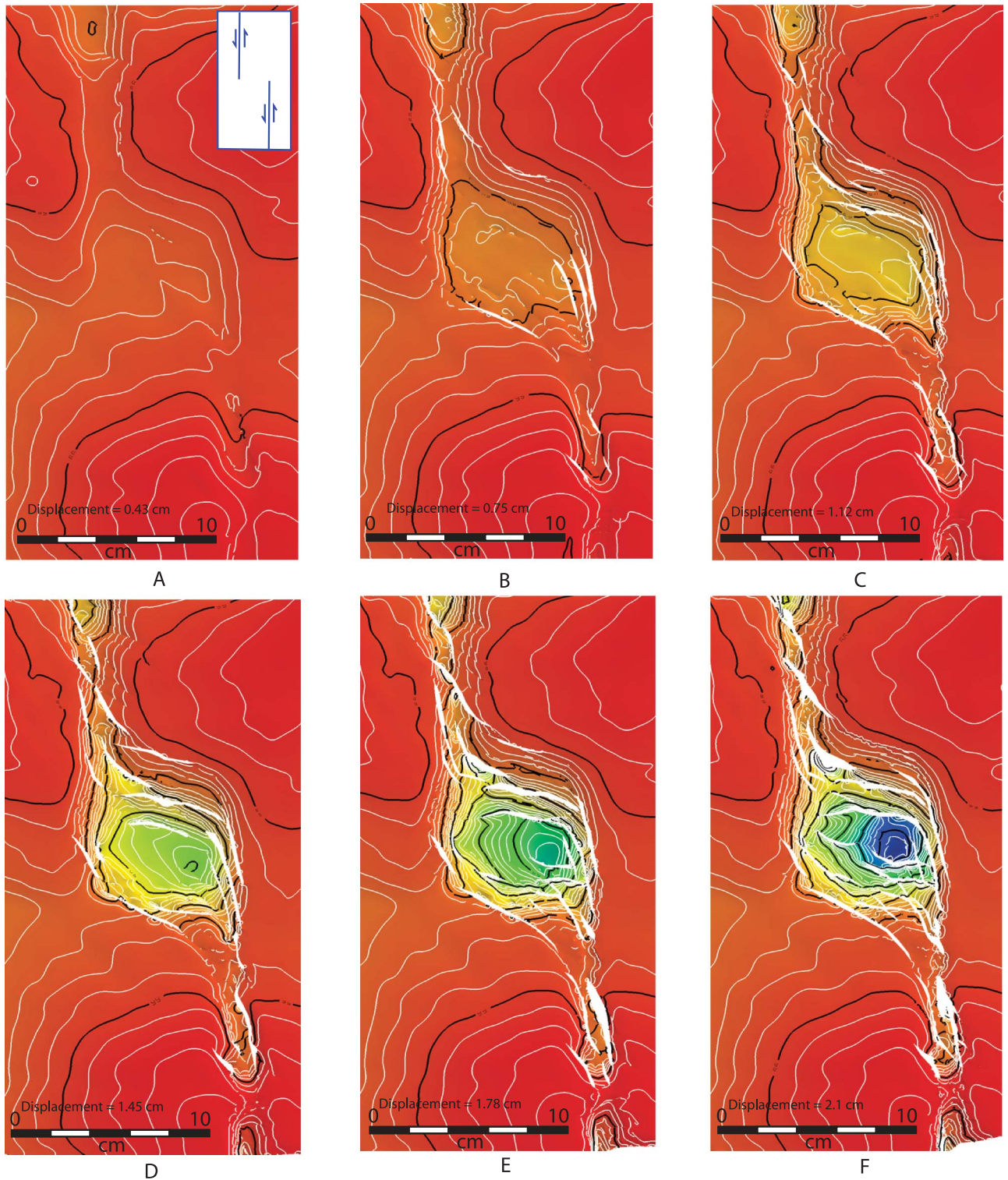
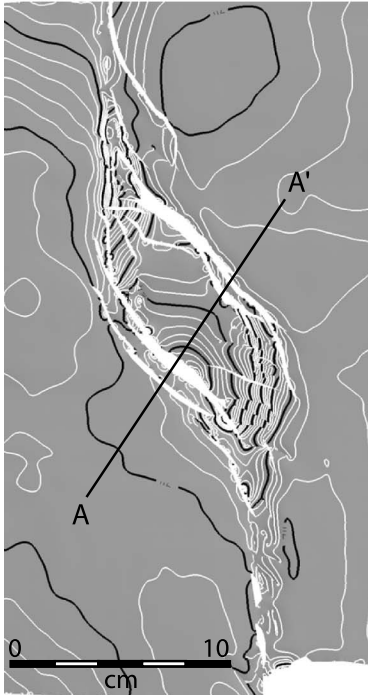
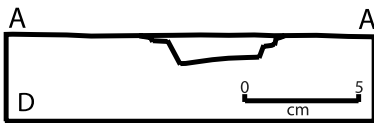


Figure 9. Three-dimensional geometry of the top of the sedimentary cover for a releasing offset with a transverse (90°) offset between two strike-slip fault segments in the basement. Panels A–F show the progressive evolution of the structure with increasing strike-slip displacement.

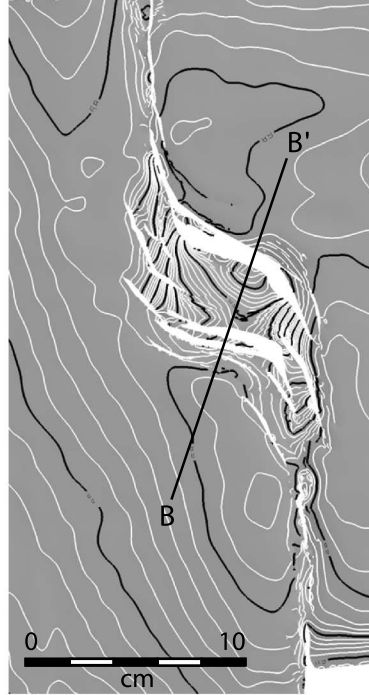
Spindle Shape



A Oblique 45° Bend



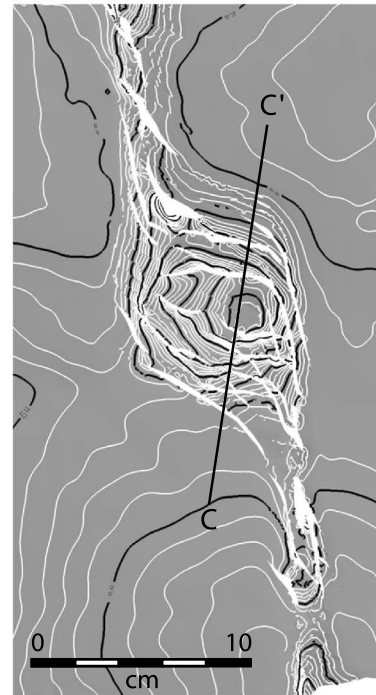
S - or Rhomboid Shape



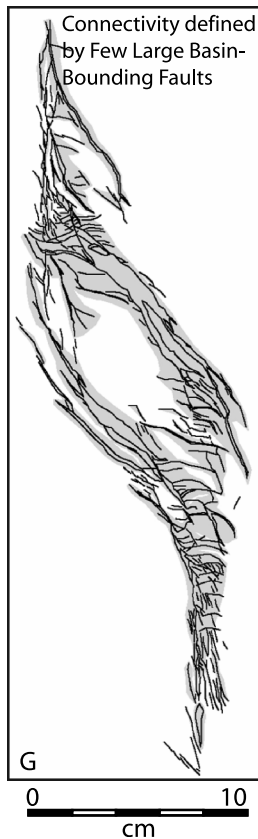
B Transverse 90° Bend



S - or Rhomboid Shape



C Transverse 90° Offset



deformation, some of the normal faults propagate laterally and connect with the R shears to form sigmoidal fault systems (Figures 8C–F, 9C–F).

The final geometry is defined by a larger number of small faults in the transfer zone compared with the experiments involving bends (Figures 8F, 9F). The reason for this difference is that the basement deformation is distributed over a wider zone than along a single connecting bend. The horizon contours are discontinuous and terminate along the faults. The faults show a complete range of distributions from north–northwest to west–northwest (Figure 8F). The deepest part of the basin is formed in the northeast corner of the pull-apart basin. Again, we attribute this to the distribution of slip among the faults, instead of the experimental configuration.

Comparison of Pull-Apart Geometries for Different Experimental Configurations

Panels A to C of Figure 10 show the final geometries of the oblique bend, transverse bend, and transverse offset configurations, with approximately the same amount of strike-slip deformation. Cross sections through the basin are shown in Figure 10D to F. The main differences in the geometries of the structures and the faults are that (1) an oblique bend results in a spindle-shaped basin, whereas a transverse bend or offset result in more S-shaped or rhomboid-shaped basins; (2) the bend configuration results in a narrower and deeper basin with fewer normal faults that accommodate the extension, whereas the offset configuration results in a wider and shallower basin with a transfer zone consisting of a large number of faults; (3) the connectivity of faults is defined by fewer longer faults for the connected setup, whereas the offset configuration results in a more diffuse connected zone defined by a large number of shorter faults (Figure 10G–I);

and (4) the deepest part of the basin is located in different locations in various experiments depending on the symmetry of the basin and the distribution of slip among the different faults. In all cases, it was found that the central parts of the faults went through minimum rotation, whereas their margins were rotated considerably into the strike-slip zones with ongoing deformation, especially in the transverse bend and offset experiments.

Comparison with Previous Models of Releasing Bends

Several sand and clay models of releasing bends have been published in the past (Dooley and McClay, 1997; Rahe et al., 1998; Basile and Brun, 1999; Atmaoui et al., 2006; Wu et al., 2009). The current models have several similarities and some key differences with past models, in the experimental setup, and boundary conditions, analysis, and results. The results of the models should be considered as complementary to those in previous studies.

Most the past experiments used sand to represent the sedimentary units and rigid sliding plates to represent the basement. The basement was therefore modeled as perfectly rigid and unable to deform. Our experiments use a two-layer model, driven by basal sliding plates, in which the basement is represented by stiff clay, whereas the sedimentary cover is represented by soft clay.

This configuration enables us to model both bends and offsets for pull-apart basins and compare the differences. Furthermore, it allows for basement deformation in the vicinity of the faults.

Several sand models (Dooley and McClay, 1997; Basile and Brun, 1999; Wu et al., 2009) used fills to study syngrowth sediments. Serial sections were used by Dooley and McClay (1997), Wu et al. (2009), to study cross sectional fault geometries. The focus of our studies was the structural relief of

Figure 10. Comparison of final geometries and fault patterns for three releasing bend and offset experiments, with approximately the same amount of strike-slip deformation. (A) Oblique (45°) bend in basement fault. (B) Transverse (90°) bend in basement fault. (C) Transverse (90°) offset in basement fault. Note the smaller angle between normal faults and main strike-slip faults leading to a spindle shape in (A) compared with the higher angle leading to an S or rhomboid shape in (B) and (C). Also the extension is distributed among fewer major faults and a smaller area in (A) and (B) compared with (C). (D–F) Cross sections through the top of the clay showing the final basin geometry for the three experiments. Locations of the cross sections are shown in (A) to (C). (G–I) Fault connectivity in the three model configurations. Note that in (G) and (H), the connectivity is controlled by fewer large basin-bounding faults, whereas in (I), the connectivity is distributed over a larger number of smaller faults.

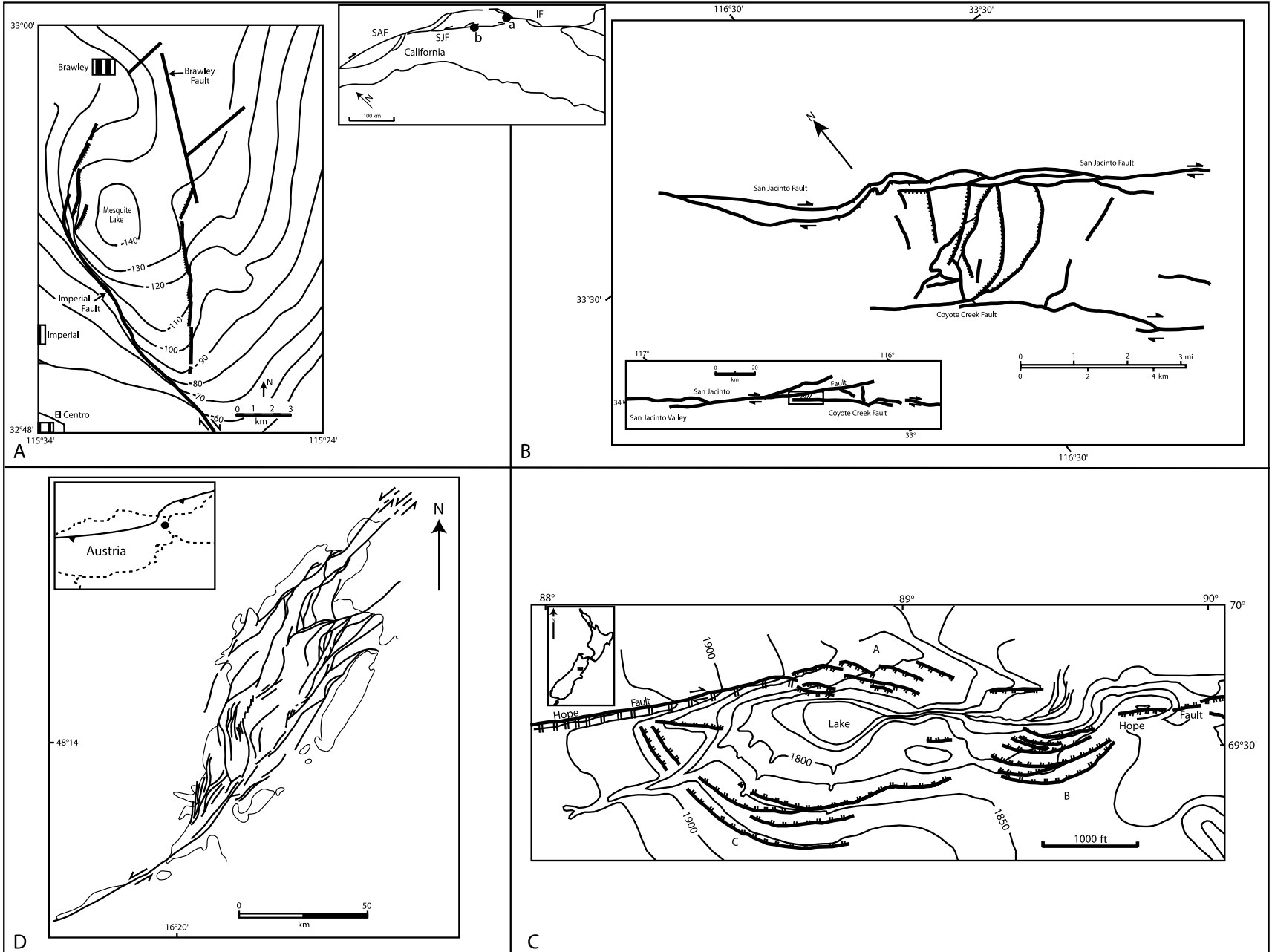


Figure 11. Examples of releasing bends and offsets. (A) Right-stepping releasing offset between the Imperial and Brawley faults in the Imperial Valley, California (redrawn from Johnson and Hadley, 1976, used with permission from the Seismological Society of America). The major faults are right-lateral strike-slip faults. The Mesquite Basin marks the deepest part of the basin. The area was the site of the 1975 Brawley earthquake. Inset shows location of (A) and (B). IF = Imperial fault. SAF = San Andreas fault. SJF = San Jacinto fault. (B) Transfer zone between the Clark and Coyote Creek right-lateral strike-slip faults in the San Jacinto fault zone (modified from Sharp, 1967, 1975, used with permission from the California Geological Survey). The area of overlap between the two faults is marked by a series of normal faults that trend at a high angle to the strike-slip faults. (C) Right-stepping offset in the right lateral Hope fault, South Island, New Zealand (modified from Clayton, 1966). The offset results in the formation of a pull-apart basin, whose deepest point is marked by a glacial lake. (D) Map of the Vienna Basin showing major faults (from Royden, 1985, used with permission from SEPM). Strike-slip faulting is distributed along a number of left-lateral faults that are interpreted to lose their strike-slip component and branch into a series of en echelon normal faults in the basin.

units and their relationship to faults, as represented by structure contour maps, to enable a direct comparison with natural structures.

For releasing bends, the detailed fault geometries and their kinematic evolution are somewhat different from those in the previous studies. Dooley and McClay (1997) documented two primary Riedel shears that developed increasing normal separation with ongoing deformation and eventually curved into the primary strike-slip orientation to define the boundaries of the pull-apart basins. Late-stage strike-slip faults parallel to the bounding strike-slip faults (Y shears), oblique strike-slip faults traversing the pull-apart basins, and a few secondary faults of other orientations were also documented. Similar results were documented by other authors. Atmaoui et al. (2006) and Basile and Brun (1999) also documented the formation of some R' shears with progressive deformation. Our results show the separate formation of R Riedel shears in the vicinity of the basement faults, the simultaneous formation of multiple sets of oblique normal faults in the central part of the basin, and the eventual conjunction of these fault sets to result in the distinct S-shaped geometries of pull-apart basins. They also show the formation of R' shears at high angles to the faults, Y shears, and oblique strike-slip faults in the late stages of deformation. Overall, the number of fault sets and density of faults documented are generally higher than in the sand experiments. The relative densities of the faults and the progressive evolution of the relative densities are also documented in our studies.

Dooley and McClay (1997) showed the transition from spindle or S-shaped geometries in oblique approaching bends to more rhomboidal geometries in the transverse or oblique overlapping bends, and similar results are obtained in our study. In our experiments, this transition is accompanied by increasing curvatures in the faults within the basin, resulting from the larger differences in the orientations of the normal faults and R Riedel shears.

The two-layer models in this study document the difference in geometries between releasing bends and offsets in the basement faults, which have not been previously modeled. The primary difference is that the pull-apart basin consists of a

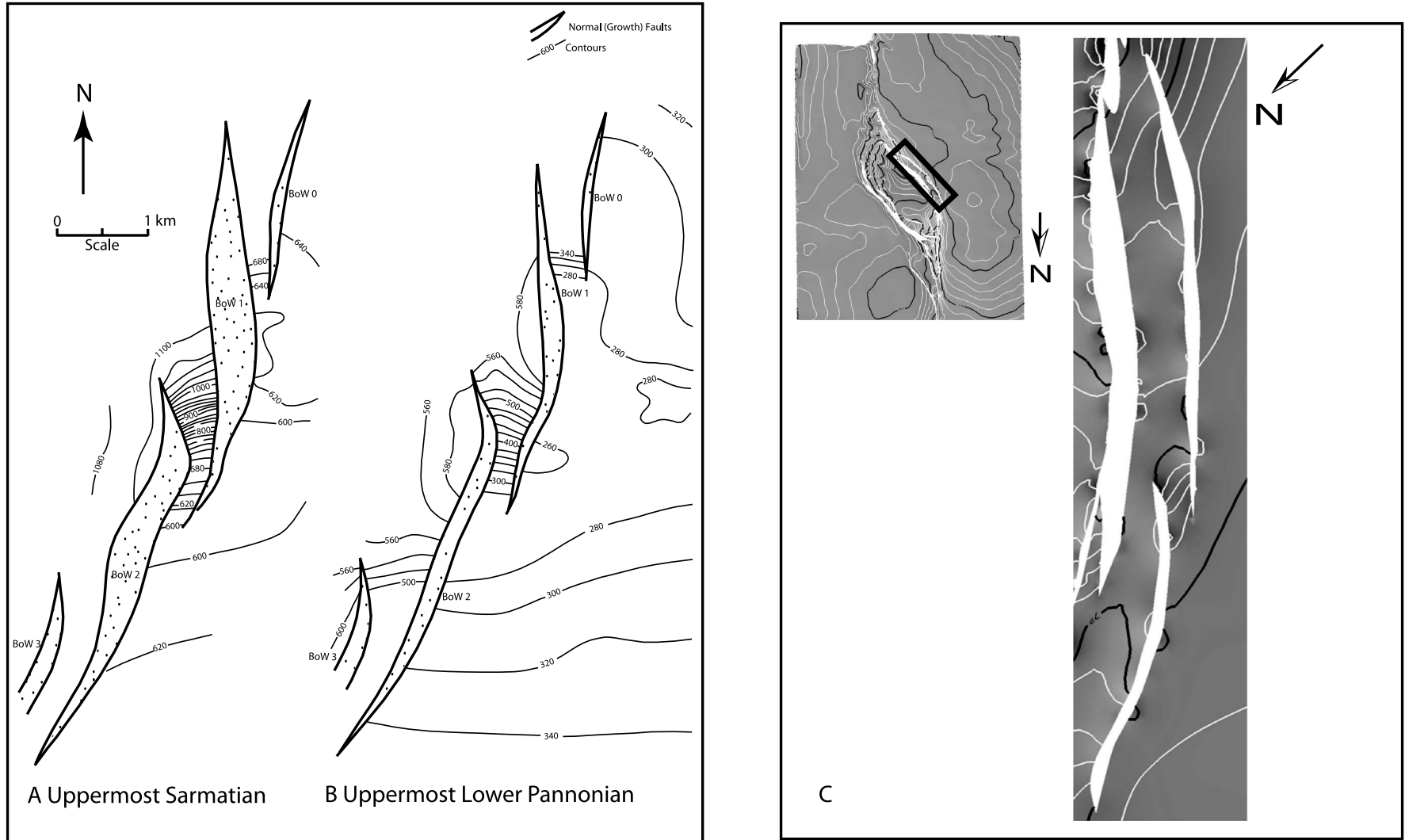


Figure 12. (A, B) Details of the Bockfleiss faults in the Vienna Basin, mapped on the basis of subsurface data (from Wessely, 1988; reprinted with permission from AAPG). Faults show increasing heave in lower horizons because of growth (compare A with B). Faults exhibit a typical en echelon and sigmoidal geometry and are separated by ramps, with contours at high angles to the faults. This pattern is typical of faults formed in pull-apart basins as seen in the experimental model for an oblique bend or offset in (C) (see inset for location of faults).

larger density of faults. In addition, using deformable stiff clay to model the basement, different shapes of the resulting basins are modeled (Figure 10). In particular, basins resulting from releasing offsets result in a smoother shape of the top of the basement, as depicted in the map and cross section in Figure 10C and F because the basin shape is defined by a large number of low displacement faults.

NATURAL EXAMPLES OF RELEASING BENDS AND OFFSETS

Surface exposures of structures formed along releasing bends provide the best natural analogs for comparison with the experimental analogs because the details of the fault patterns and orientations can be studied in detail. The experimental models and the surface models can be used to interpret subsurface examples of these structures, for which more limited data are available. The following well-documented surface examples provide a suite of structures that can be compared with the observations in the experimental models.

Imperial and Brawley Faults, Imperial Valley, California

The Imperial and Brawley faults make up a right-stepping releasing bend or offset on a set of right-lateral faults in the Imperial Valley California (Johnson and Hadley, 1976). The transfer zone between the two faults is primarily marked by two well-defined sets of en echelon normal faults, which curve toward each other (Figure 11A). The faults originating at the Brawley fault make a smaller angle to the main fault ($\sim 11^\circ$), whereas those originating at the Imperial fault make a higher angle (closer to 52°). The area was the site of the Brawley swarm of earthquakes in 1975. The earthquakes originated on the Brawley fault and migrated both north and south on the fault and also occurred on additional faults in the area of the transfer zone. Comparison with the experimental evolution suggests that the earthquakes formed along newly developing fault segments within the transfer zones. The Mesquite Basin, which marks the depocenter within the

pull-apart basin, is located closer to the northwest boundary of the basin, suggesting an asymmetric flexure within the basin. The low density of faulting and the presence of short unconnected fault segments suggest that this configuration represents an early stage of a releasing bend or offset between approaching faults.

San Jacinto–Coyote Creek Faults

The San Jacinto strike-slip fault zone is characterized by several en echelon strands (Sharp, 1967, 1975). One of the transfer zones between the San Jacinto (Clark) and Coyote Creek faults is well exposed in the area to the north of the Coyote Canyon (Figure 11B). The transfer zone is marked by an overlap between the two faults. The area of overlap contains several northeast-trending and northwest-dipping normal faults. These faults, although showing some strike curvature at their boundaries, show an almost normal trend relative to the bounding strike-slip faults. The dips of the faults shallow with depth (Sharp, 1975). Sharp (1967) has suggested that the total crustal extension has not exceeded about 2.5 km (1.6 mi), which he postulates to be the net right-lateral slip on the northern part of Coyote Creek fault. Our experimental models suggest that the geometries in the San Jacinto–Coyote Creek transfer zone are related to the fact that lateral and overlapping transfer zones are marked by increasing angles of the connecting normal faults to the bounding strike-slip faults.

Hope Fault, Glen Wye, New Zealand

The Hope fault is the southern element of the Marlborough fault system, a major right-lateral strike-slip fault located on South Island, New Zealand (Clayton, 1966; Cowan, 1990). In the vicinity of the Glen Wye area, offset Pleistocene glacial moraines and river terraces indicate predominant right-lateral motion (Figure 11C). The area is also marked by a major releasing offset toward the south. The northern boundary of the pull-apart basin shows a single fault, whereas the southern boundary is made

up of several short discontinuous segments with opposite dips as seen in the early stages of the experimental models. Both of these fault systems represent the parts of the strike-slip fault where the strike-slip component diminishes significantly and a normal component dominates.

The termination of the northern strike-slip fault is marked by a zone of curved south–southwest–dipping en echelon normal faults (A), which step down toward a glacial lake in the center of the pull-apart basin. These faults have an average trend of approximately 24° to the main fault at their termination within the basin. The southern fault segment is marked by two zones of normal faults, B and C, which curve asymptotically into the main fault zone. Fault zone B consists of shorter fault segments with an average trend of 39° to the main fault and terminates at the basin margin, whereas fault zone C consists of longer faults, with an average trend of 54° to the main fault and marks the southwestern extremity of the pull-apart basin.

The multiple zones of faults, distributed over a wide area, and the discontinuous nature of these faults suggest that the basin formed along a right-stepping offset, similar to those in Figures 8 and 9.

Vienna Basin, Austria and Czech Republic

The Vienna Basin is a large pull-apart basin superimposed on the north-vergent nappes of the outer West Carpathian flysch belt and partly on the Inner Carpathian belt (Royden, 1985). The basin contains gas accumulations located in structural-stratigraphic traps within horst blocks in the Sarmatian and Pannonian units. It is one area where structural traps within the pull-apart basin can be directly studied. The Matzen field is the largest multipool field within the Vienna Basin (Kreutzer, 1992). The field produces oil and gas from multiple sand and carbonate reservoir units in a complexly faulted structure.

The detailed structure and evolution of the basin has been documented in detail by Royden (1985). During and after the Badenian, synsedimentary growth faults with large throws formed (Wessely, 1988). The basin formed between two left-stepping segments of left-lateral strike-slip

faults. The main strike-slip fault segments separated thrust faulting in the area east of the basin from already thrust-faulted areas to the west. Royden (1985) has proposed that the strike-slip faults and related normal faults detach within a southeast dipping detachment at depth, so that extension and strike slip is restricted mainly to shallow crustal levels, whereas Wessely (1988) has suggested that the extension may extend into the autochthonous units underlying the allochthonous thrust sheets. Evidence to compare and evaluate these alternative models is not apparent in the surface data through the basin.

The detailed structure of the basin is depicted in Figure 11D. The basin is bounded by two main strike-slip faults, both of which lose slip as they approach the basin and eventually curve into the pull-apart basin. A third strike-slip fault is located in the central part of the basin. Royden (1985) has suggested that the main active segments of the faults may have changed somewhat over time, but that the total slip was distributed along these major faults and a large number of smaller faults. Regionally, the area of the offset is marked by a large number of en echelon normal fault segments. These fault segments curve asymptotically as they approach the main strike-slip segments.

The details of the normal faults have been studied by Wessely (1988) based on extensive well data in the basin. Several phases of faulting occurred in the basin. The late Miocene (Badenian and younger) faults, which formed after thrusting and during the basin evolution typically maintain a constant dip of 40 to 50° (Wessely, 1988). Among these, the Bockfleiss faults located in the western part of the basin show typical en echelon geometry and sigmoidal shapes and progressively drop each unit down into the deeper part of the basin (Figure 12A, B). Because the faults are synsedimentary growth faults, they also show larger throws and heaves in deeper units. At the transfer zones between the faults, contours are typically closely spaced and at a high angle to the fault trends, as also seen in the experimental models (Figure 12c). The multiple normal faults suggest a complex faulted basin formed along one or more transverse or approaching offsets between two or more strike-slip faults.

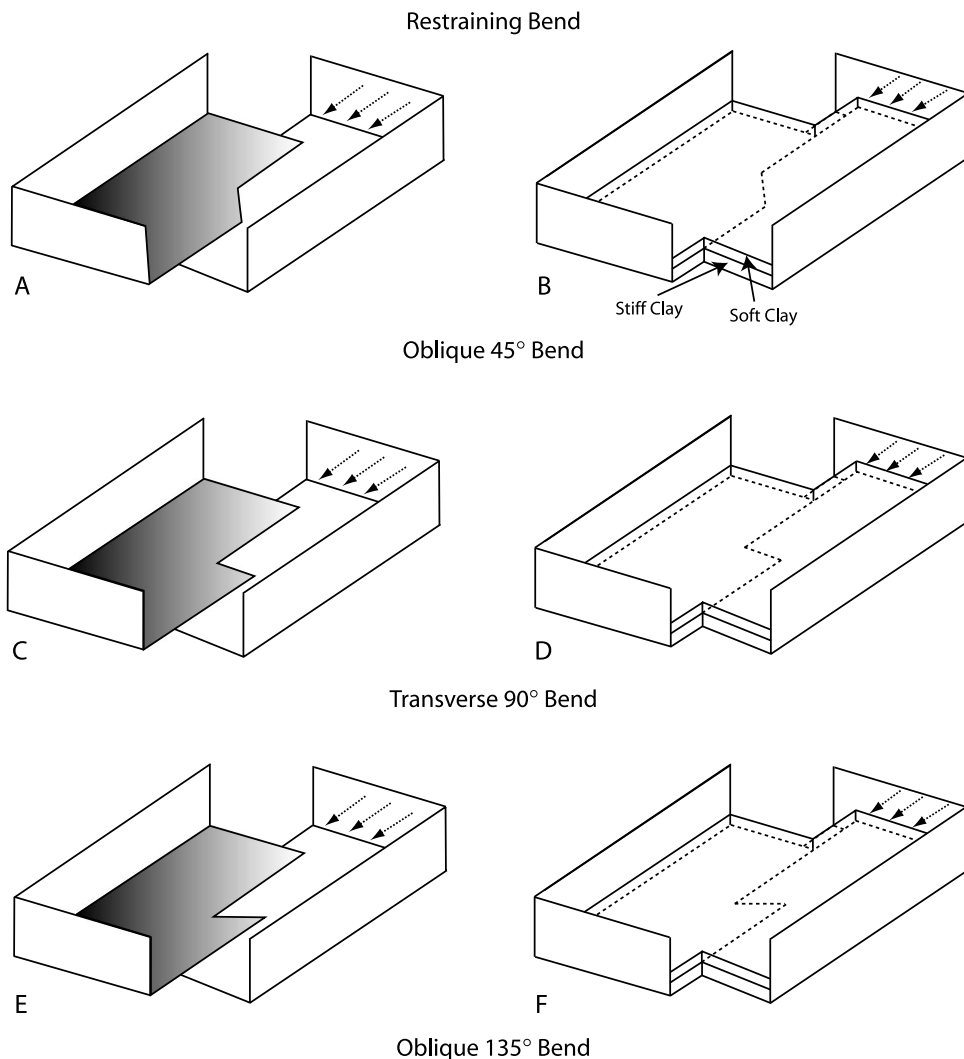


Figure 13. Experimental models conducted for restraining bends. (A, B) Oblique 45° bend in basement fault. (C, D) Transverse 90° bend in basement fault. (E, F) Oblique overlapping 135° bend in basement fault. For each experiment, the first figure shows the relationship between the underlying sliding plates, and the second figure shows the two clay layers and the preexisting fault cuts in the basement.

RESTRAINING BENDS

Experimental Approach

The experimental configuration used for restraining bends is similar to that for releasing bends, except that convergence between the metal plates is used to create right-lateral shear (Figure 13). The overlying stiff and soft clay layers are deformed during the convergence between the metal plates. Similar rates of movement are used as for the releasing bends. Vertical cuts in the stiff layer are made directly above the boundaries between the metal plates to represent the initial positions of the basement strike-slip faults. Only bend configurations yield the optimum configurations for compressive structures to form in the transfer zone.

Therefore, only bend configurations are investigated in the final configurations. Oblique (45°), transverse (90°), and oblique (135°) bend configurations are all modeled (Figure 13).

The fault geometries are traced directly from photographs taken during successive stages of the experiment. In addition, laser scans are used to model the structures and fault geometries on the top clay surface.

Experimental Results

Oblique (45°) Bend

Right lateral slip on a 45° restraining bend results in the formation of an elongate fold at an angle of approximately 36° to the main strike-slip faults (Figures 14A, B; 15A, B). All measurements for

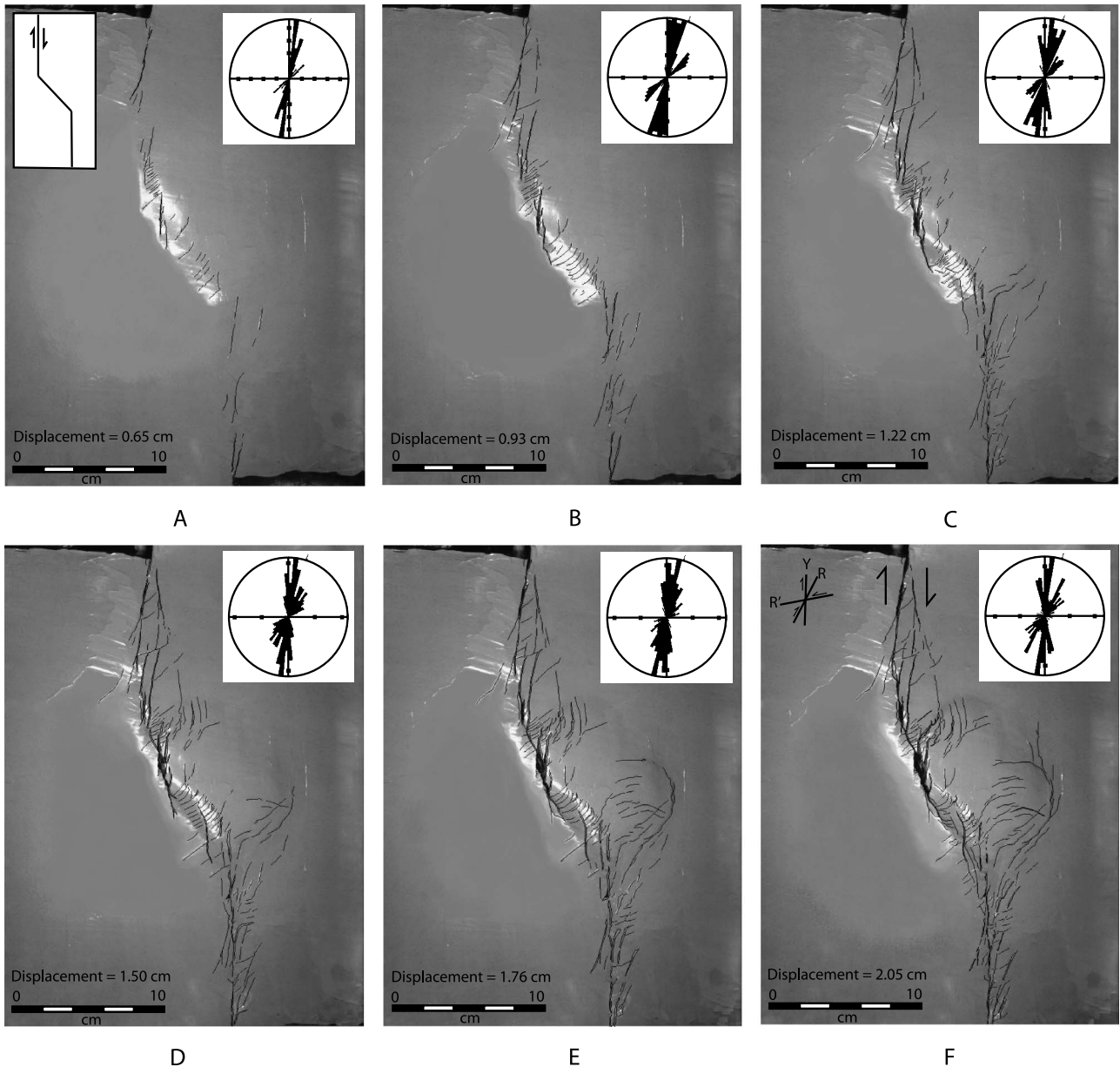


Figure 14. Clay models showing faults in the sedimentary cover for a restraining bend with an oblique (45°) bend connecting two strike-slip fault segments in the basement. Sense of slip on the strike-slip faults is right lateral. Panels A–F show the progressive evolution of the structure with increasing strike-slip displacement. Rose diagrams show the lengths of faults for different trends in 5° increments as a percentage of the total length of faults.

the restraining bends are made in a clockwise direction from the main strike-slip faults. The structural high is cut by several fractures or normal faults, which are oriented approximately normal to the axis of the structure. Immediately above the main strike-slip segments, a series of en echelon faults form at angles of 8 to 18° to the basement strike-slip faults. These faults are interpreted as R

Riedel shears emanating from the basement strike-slip faults. With progressive deformation, the fold becomes more asymmetric verging to the southwest and develops some northeast-dipping reverse faults parallel to the structural trend especially along the steep southwest limb of the structure (Figures 14C, D; 15C, D). In the final stages, the structure grows broader and attains its greatest

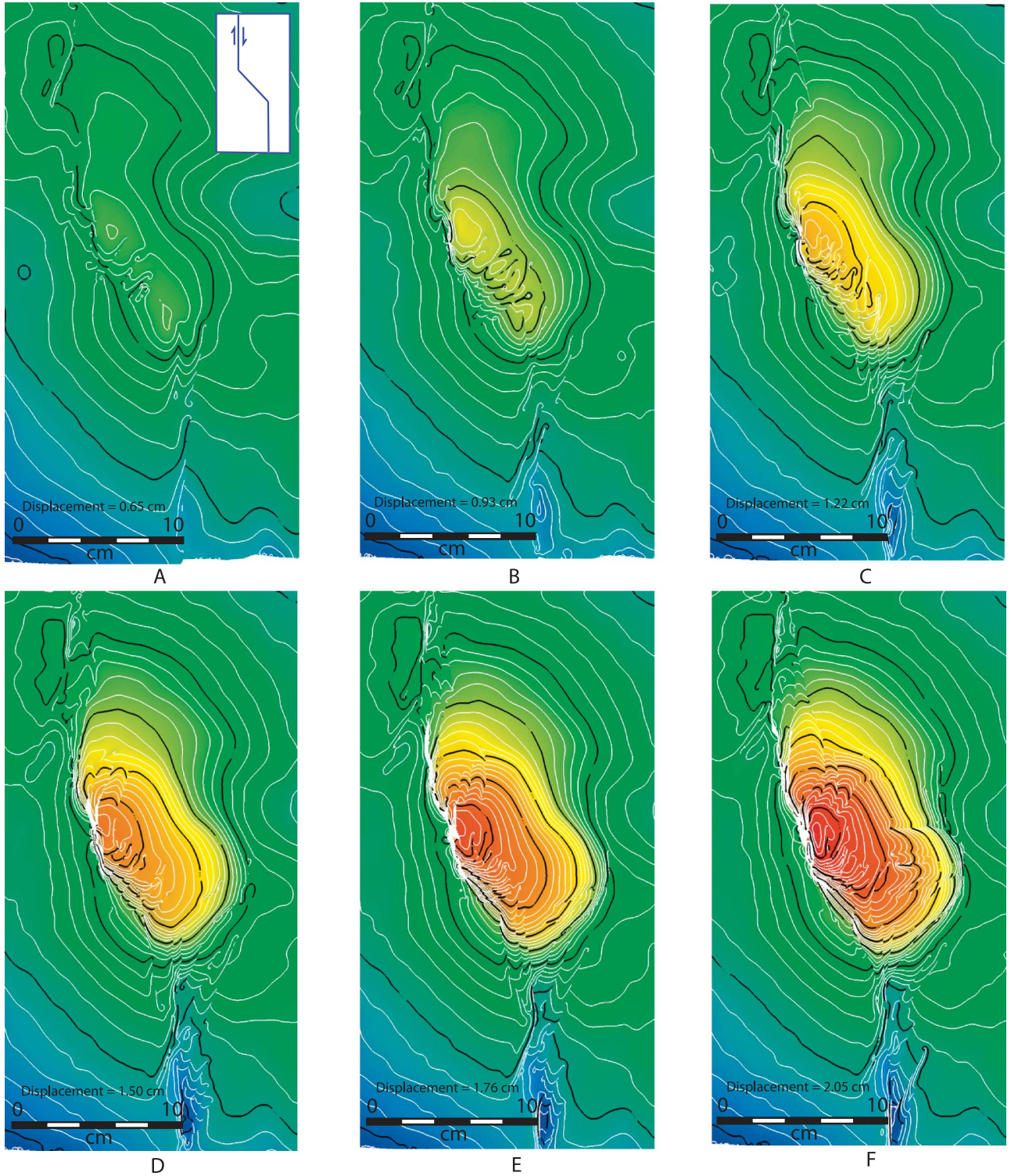


Figure 15. Three-dimensional geometry of the top of the sedimentary cover for a restraining bend with an oblique (45°) bend connecting two strike-slip fault segments in the basement. Panels A–F show the progressive evolution of the structure with increasing strike-slip displacement.

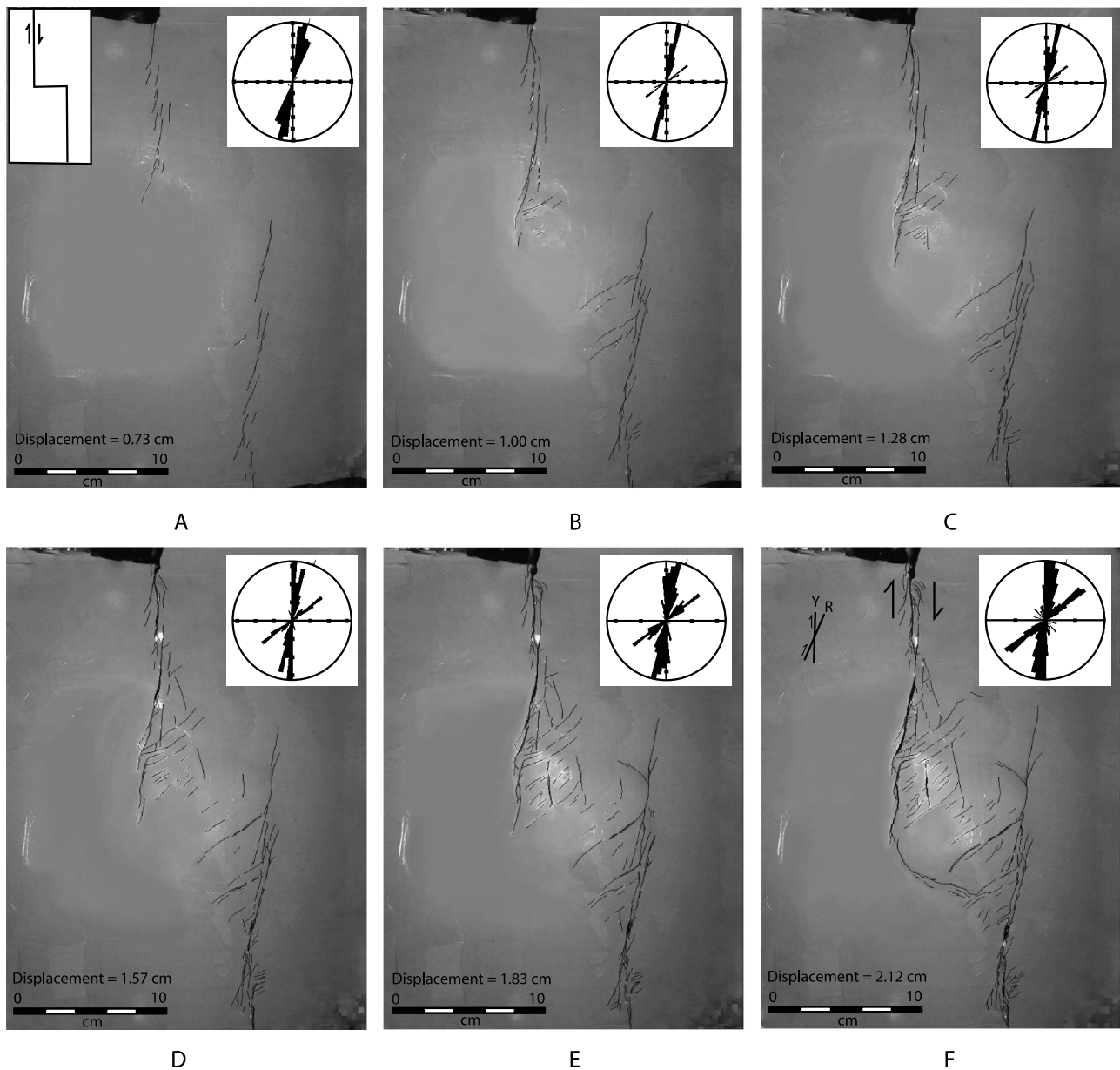


Figure 16. Clay models showing faults in the sedimentary cover for a restraining bend with a transverse (90°) bend connecting two strike-slip fault segments in the basement. The sense of slip on the strike-slip faults is right lateral. Panels A-F show the progressive evolution of the structure with increasing strike-slip displacement. Rose diagrams show the lengths of faults for different trends in 5° increments as a percentage of the total length of faults.

structural relief. It also shows a small clockwise rotation, with the central part trending approximately 26° to the main strike-slip faults in the final stage (2.05 cm of displacement). Linear strike-slip faults, parallel to the main faults (Y shears), also break through the sedimentary cover and bound the structure on two sides (Figures 14E, F; 15E, F). Some

curved faults at a high angle to the Y shears, which are possible R' shears, form at the terminations of the main faults.

The faults exhibit five dominant trends, north, north-northeast, and west-trending strike-slip faults, north-northwest-trending reverse faults, and the northeast-trending normal faults (Figure 14F).

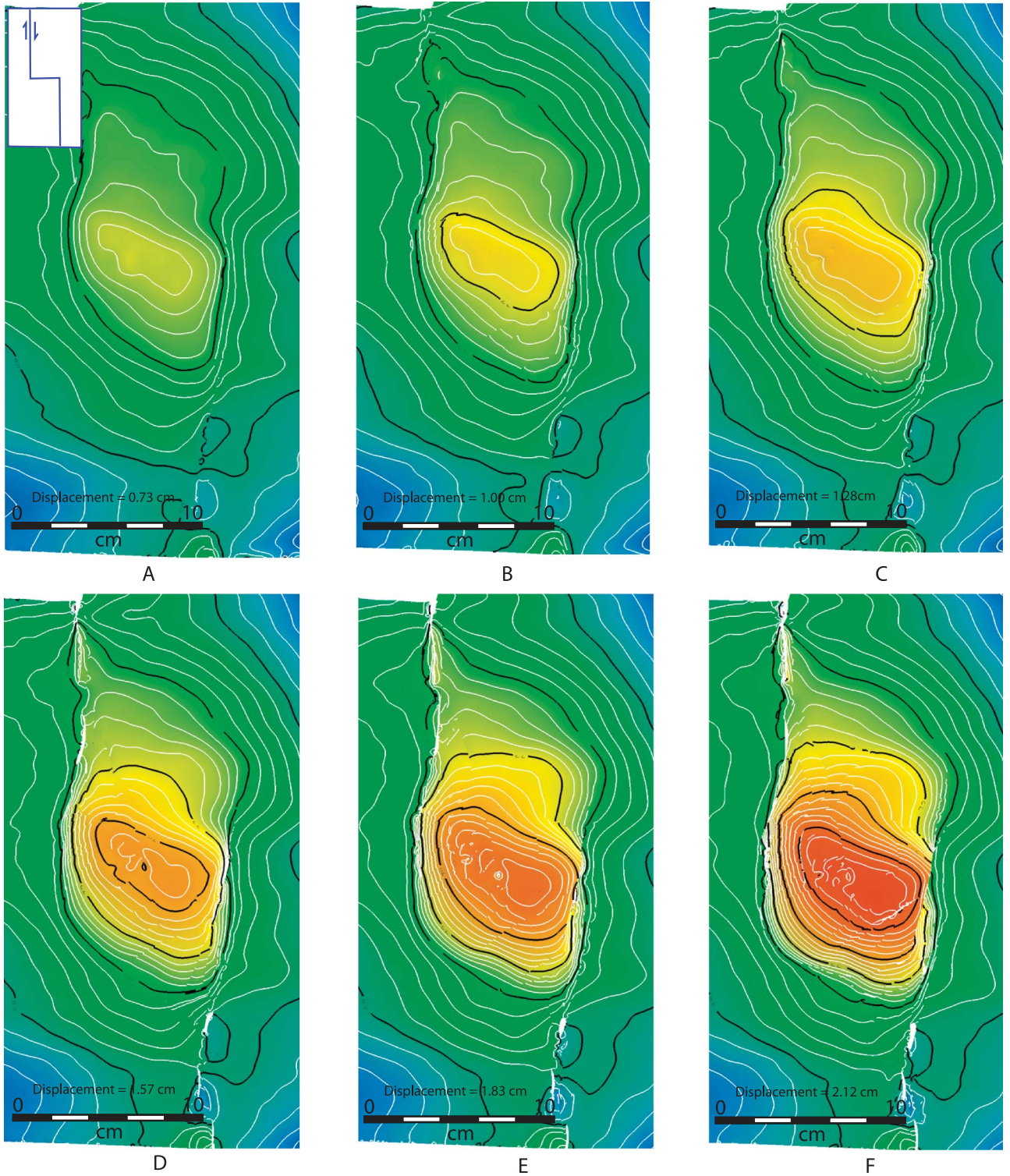


Figure 17. Three-dimensional geometry of the top of the sedimentary cover for a restraining bend with a transverse (90°) bend connecting two strike-slip fault segments in the basement. Panels A–F show the progressive evolution of the structure with increasing strike-slip displacement.

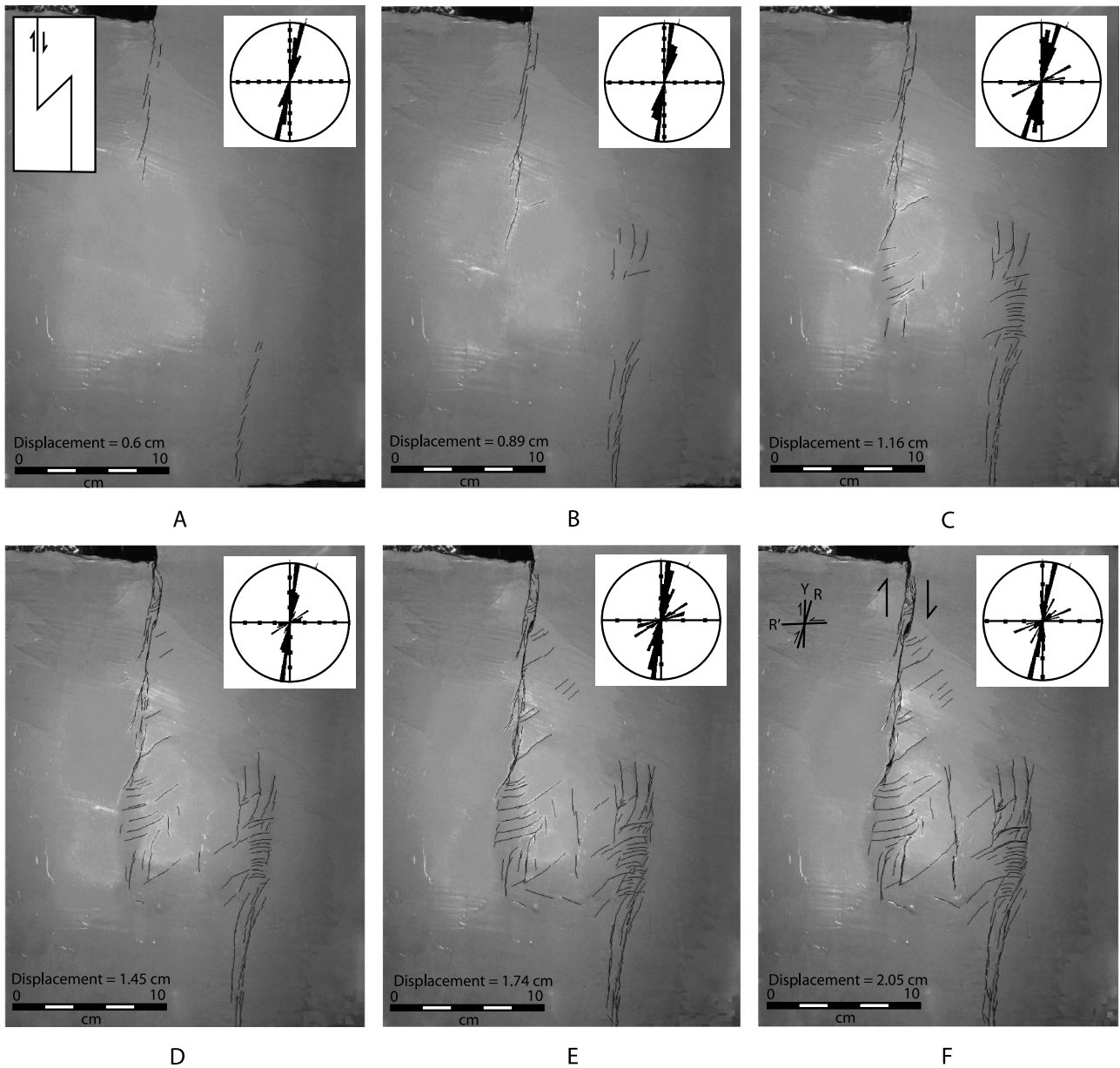


Figure 18. Clay models showing faults in the sedimentary cover for a restraining bend with an oblique overlapping (135°) bend connecting two strike-slip fault segments in the basement. The sense of slip on the strike-slip faults is right lateral. Panels A–F show the progressive evolution of the structure with increasing strike-slip displacement. Rose diagrams show the lengths of faults for different trends in 5° increments as a percentage of the total length of faults.

Transverse (90°) Bend

For a transverse (90° bend) connecting the two strike-slip fault segments, initial strike-slip results in the formation of a structural high, whose structural axis is at a high angle ($\sim 57^\circ$) to the basement strike-slip faults (Figures 16A–C, 17A–C). A series of echelon faults (Riedel R shears) forms immediately above the basement strike-slip faults at an angle of

10° to the trend of the basement faults. These faults bound the structure to the west and east. The noses of the structures also develop a series of normal faults, trending approximately 65° relative to the axis of the structure.

With increasing strike slip (Figures 16D–F, 17D–F), the normal faults also propagate to the culmination of the structure, maintaining their oblique

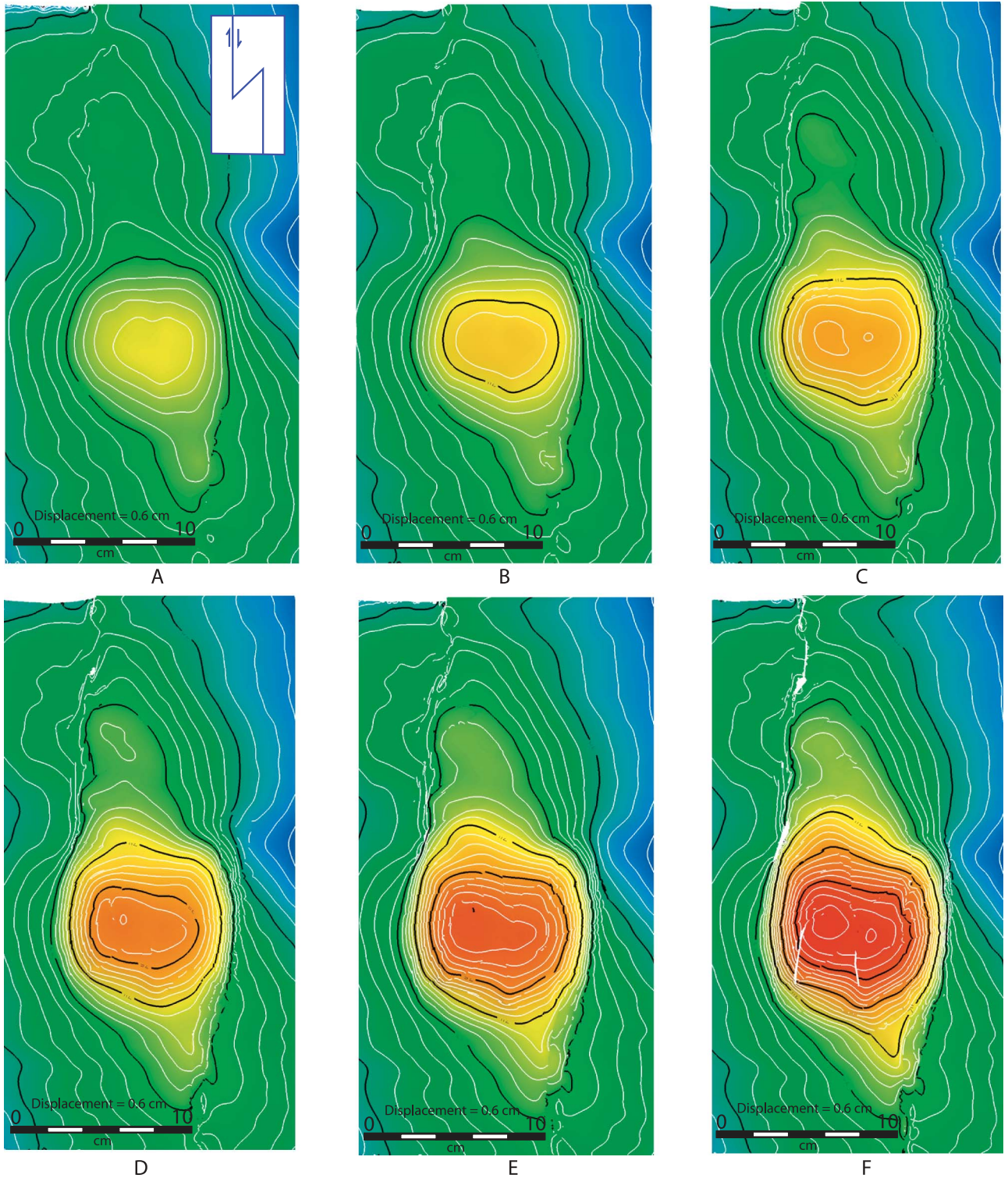


Figure 19. Three-dimensional geometry of the top of the sedimentary cover for a restraining bend with an oblique overlapping (135°) bend connecting two strike-slip fault segments in the basement. Panels A–F show the progressive evolution of the structure with increasing strike-slip displacement.

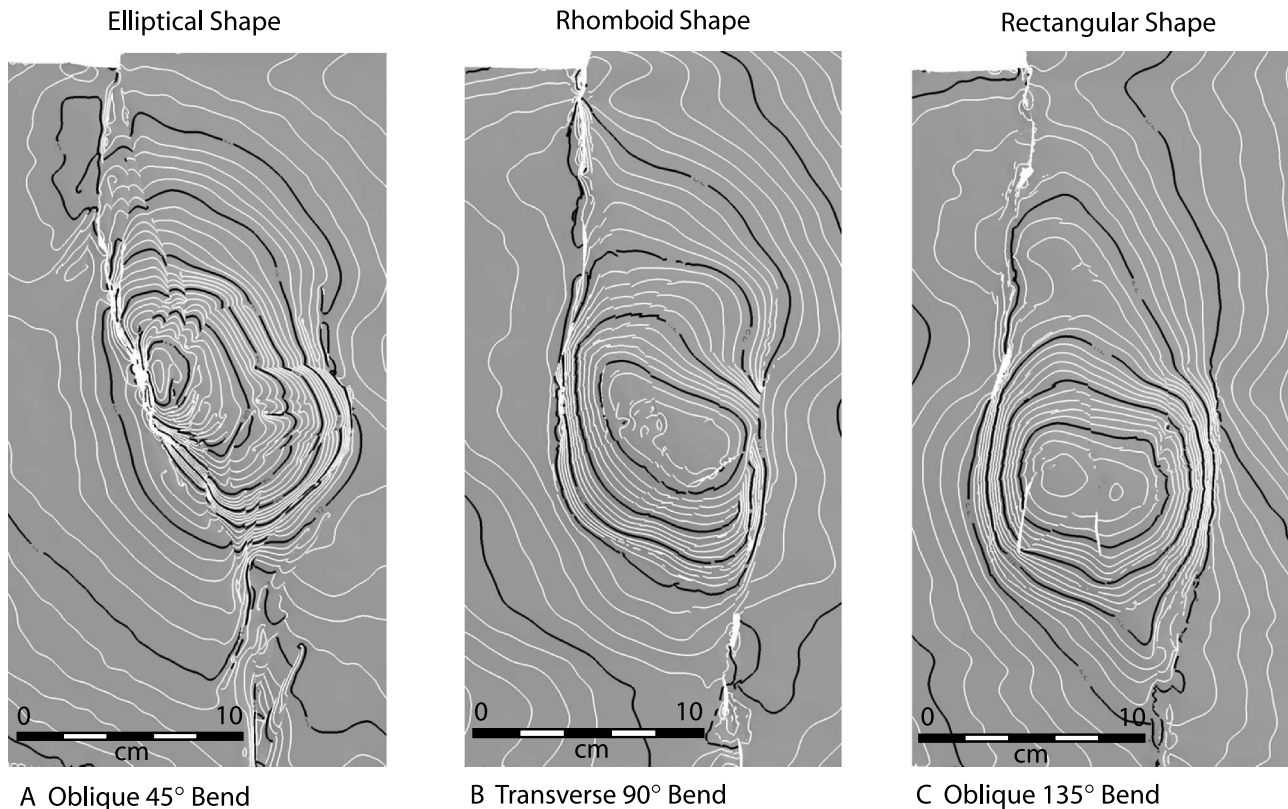


Figure 20. Comparison of final geometries and fault patterns for three restraining bend experiments, with approximately the same amount of strike-slip deformation. (A) Oblique (45°) bend in basement fault. (B) Transverse (90°) bend in basement fault. (C) Overlapping oblique (135°) bend in basement fault. Note the lower angle between axis of the structure and the main strike-slip faults leading to a more elliptical shape in (A) compared with the higher angle leading to a rhomboid shape in (B) and rectangular shape in (C).

trend. The structure is bounded by the strike-slip faults on the western and eastern flanks and broadens with increasing strike-slip, developing a rhomboid shape. The axis of the structure also curves into the strike-slip faults at both ends. In the very final stages, a pair of curved reverse faults bound the structure on the northeast and southwest flanks (Figure 16F). The main strike-slip faults also break through to the surface, forming north-south-trending Y shears. A few scattered north-northwest-trending strike-slip faults also develop. The axis of the structure in the central part rotates clockwise to make an angle of 50° with the main strike-slip faults in the final stage (2.12 cm [0.83 in.] of displacement).

Four main trends of faults are present in the final stage: a north-northeast trend for the en echelon strike-slip faults (R shears), a north trend for the Y shears, an approximate northeast trend for the normal faults, and a weak northwest trend for the reverse faults (Figure 16F).

Oblique Overlapping (135°) Bend

An oblique 135° bend signifies a scenario where the two basement fault segments have significant overlap and are connected along an oblique jog. In this setting, the structure initially forms almost at right angles to the main strike-slip faults. We consider this the least common of the three configurations modeled in the experiments because a connecting oblique jog with an acute angle or a transverse jog is likely to develop before the development of an overlap of the two basement strike-slip faults.

Initial deformation results in the formation of a structural high whose central part is almost transverse to the trend of the basement strike-slip faults. A series of en echelon strike-slip faults (R shears) form above the basement strike-slip faults at an angle of 5 to 10° and curve away from the central structure (Figures 18A–C; 19A–C). Continuing deformation results in the formation of a set of faults trending 75° (R' shears) that curve into the structure

from the strike-slip faults. Some normal faults trending obliquely (57°) to the axis of the structure also form. The ends of the structures also develop narrow segments or tails that curve into the trend of the strike-slip faults. Some of the strike-slip fault segments develop depressions, and a significant component of normal separation. In the late stages, Y shears develop above the basement strike-slip faults and a few north-northwest-trending strike-slip faults traverse the structure (Figures 18D–F, 19D–F).

The final fault pattern consists of a main trend of north-northeast-trending strike-slip faults (R shears), east-northeast-trending R' shears, north-trending Y shears, and normal faults trending north-east (Figure 18F).

Comparison of Restraining Bend Models

The three restraining bend experimental models all resulted in the formation of a central high in the bend area, two sets of en echelon strike-slip faults (R and R' shears), as well as Y shears immediately above the basement strike-slip faults (Figure 20). The structural highs all developed narrow tails that swung into the trend of the strike-slip faults. Some extension was also observed along the strike-slip fault segments in the experiments. The primary differences were that (1) the trends of the structures changed from an acute trend to the strike-slip faults for the 45° bend to an almost transverse trend for the 135° bend; (2) the normal faults formed on the structure were almost transverse to the structure for the 45° bend but oblique in the case of the transverse bend to almost parallel in the case of the 135° bend; and (3) the shapes of the structures changed from more elliptical and spindle-shaped in the case of the 45° bend to more rhomboidal or rectangular geometries with tails in the case of the transverse and 135° bends. Overall, the incidence of faulting was significantly less than for the releasing bend experiments.

Comparison of Results with Previous Models of Restraining Bends

McClay and Bonora (2001) conducted a series of sand experiments to model structures formed along restraining bends for oblique (30°), transverse, and

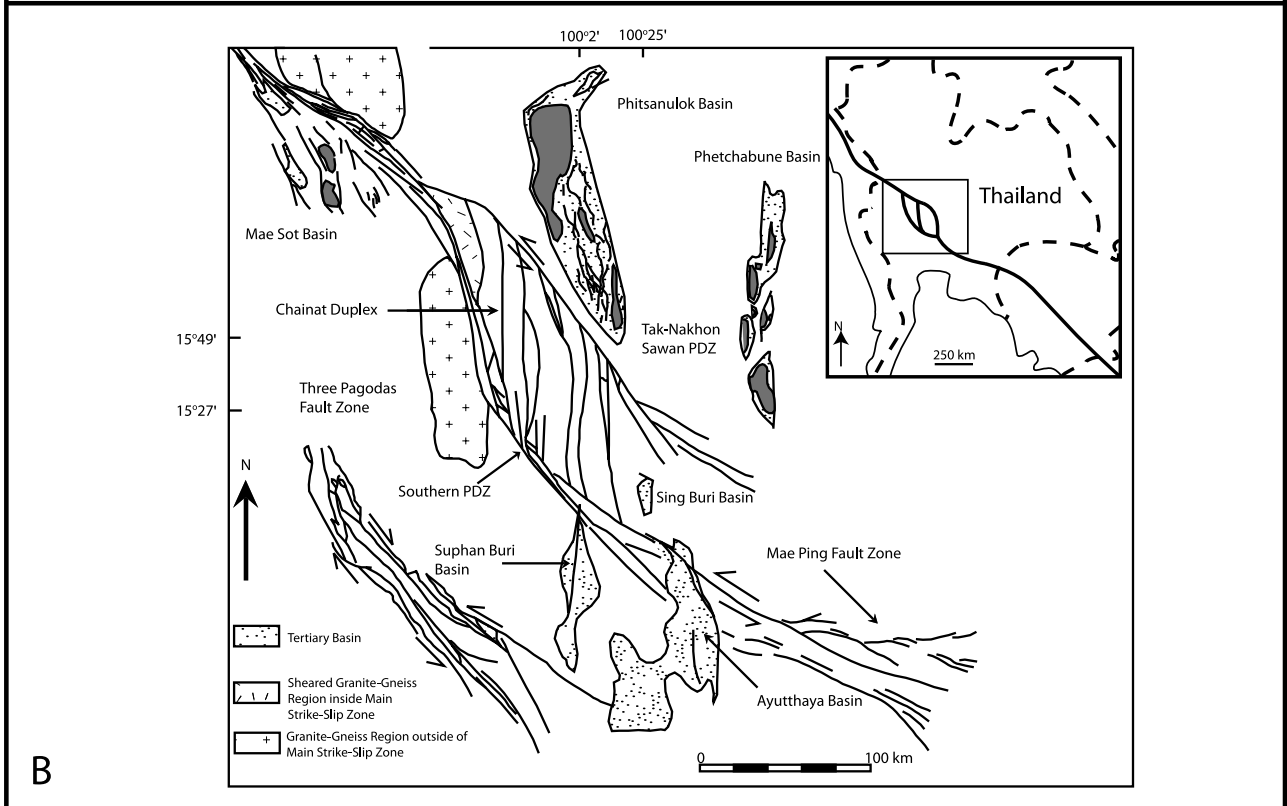
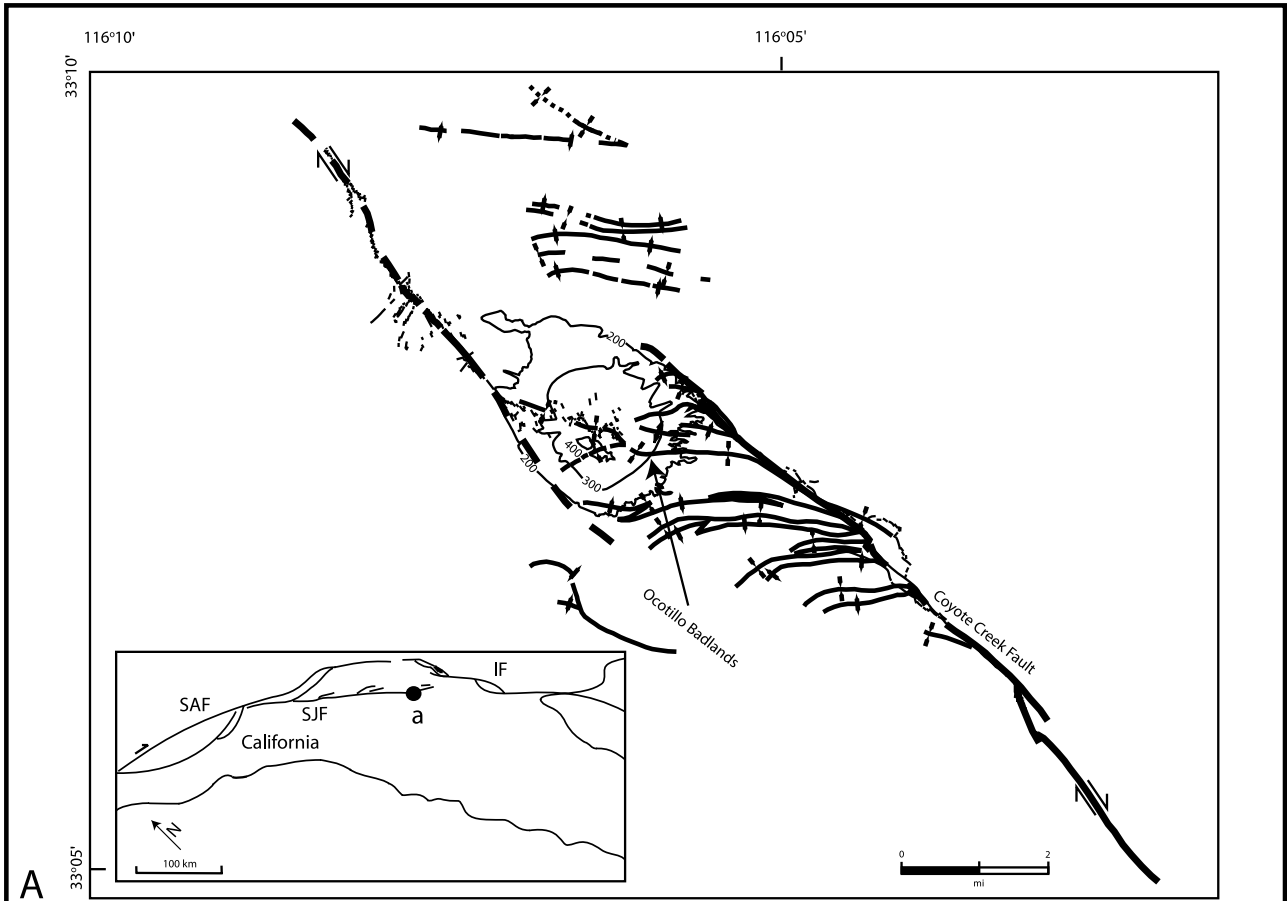
oblique overlapping (150°) cases. They studied the fault geometries with progressive evolution, the final cross sectional geometries, and the geometries of faults within sand fills. Our experiments investigate similar fault configurations but focus on the geometries of the structures using structural contour maps and the relationships of the structures to the progressively developing faults.

In McClay and Bonora's (2001) experiments, the oblique (30°) and transverse cases resulted in rhomboidal pop-up structures, whereas in the oblique overlapping (150°) case, the uplift was sigmoidal in shape. In all three cases, the maximum uplift was in the center of the stepover zone. Fault patterns included Riedel shears along the main strike-slip faults and pairs of reverse faults with strike-slip components bounding the structures. Late-stage strike-slip faults connected the two main strike-slip faults. In our experiments, the structures are asymmetric to symmetric, and partially bounded by reverse faults. The axis of the structure forms progressively higher angles in the transverse and oblique overlapping (135°) cases. The R Riedel shears are common above the main strike-slip faults, with R' and Y shears forming at later stages. In all experiments, a set of normal faults forms normal or oblique to the axis of the structures.

NATURAL EXAMPLES OF RESTRAINING BENDS

Ocotillo Badlands, Coyote Creek Fault

The Ocotillo Badlands area between segments of the Coyote Creek fault (Figure 21A) is an example of an uplift formed along a left-stepping bend or offset along a right lateral strike-slip fault (Sharp and Clark, 1972). A small overlap occurs between the two strands of the fault (Figure 21A). The area of the transfer zone is marked by a series of smaller scale anticlines and synclines, which form an acute angle averaging 37 to 40° with the main strike-slip faults. The structures curve asymptotically into the eastern fault strand. The area of greatest uplift is located in the northwestern part of the transfer zone between the two strike-slip faults.



The Borrego Mountain earthquake of 1968 resulted in rupturing on the preexisting Coyote Creek fault and related faults. The surface ruptures followed the preexisting structures and had the same sense of slip. The fine lines in Figure 21A show the locations and orientations of surface ruptures formed during and after earthquake (USGS, 1972). The locations of the surface ruptures suggest that deformation occurred both along one of the main strike slips and the evolving structures in the restraining bend. The overall structure resembles the experimental model formed along an oblique restraining bend (Figures 15, 16).

Chainat Ridge, Thailand

The Chainat Ridge uplift is located on the Mae Ping fault zone, Thailand (Smith et al., 2007). The structure has also been referred to as the Chainat duplex (Morley et al., 2007; Smith et al., 2007). The structure is approximately 100 km (62 mi) in length and formed on north-south-trending Khlong Lhan restraining bend on a predominantly northwest-south-trending left-lateral fault (Figure 21B). The area of the restraining bend is marked by a series of north-south ridges trending about 40° to the main strike-slip faults and exposing Paleozoic and Mesozoic rocks and bounded by a series of faults. The structure has been described as a gentle restraining bend and resembles the experimental model of a moderate-angle oblique jog on a strike-slip fault (Figures 15, 16). The primary difference is the number of secondary faults and structures in the example compared with the single large uplift in the experimental model. The wavelengths of folds and related faults are typically proportional to the thickness of dominant units that are involved in the deformation. Therefore, the absence of layering in the experimental models induces the for-

mation of a single large-scale structure, instead of an assemblage of smaller scale structures.

DISCUSSION AND CONCLUSIONS

Restraining and releasing bends and offsets can result in a wide array of extensional or compressive structures. The experiments described in this article document the 3-D geometries of the surface horizon and evolution of some of the more common configurations. Based on the experiments, several conclusions can be made regarding the 3-D geometry of the structures. The use of laser-scan models provides a useful tool for documenting the details of the structures in the transfer zones and their progressive evolution.

Several suggestions have been made regarding the development and subsequent evolution of the jogs in the main strike fault and related secondary structures (Crowell, 1974; Aydin and Nur, 1985). Crowell (1974) suggested that the major strike-slip faults develop bends with ongoing slip and subsequently develop a secondary branch in the area of the bend, resulting in the formation of a fault wedge between the two faults. Deformation within the wedge results in the formation of pull-apart basins or uplifts, depending on the orientation of the fault bend and the sense of strike slip. Our approach has been to introduce fault bends or offsets in the main basement faults and document the resulting patterns in the overlying sedimentary cover. For releasing bends or offsets, both connecting faults and offsets eventually result in the formation of pull-apart basins. For restraining bends, our experiments show that a connecting fault in the basement is necessary in all configurations for a well-defined structure to form in the sedimentary cover. This suggests that fault offsets

Figure 21. Examples of restraining bends. (A) Uplift formed along a restraining bend between two offset left-stepping segments of the Coyote Creek right-lateral fault in California (from Sharp and Clark, 1972). The fine lines show surface ruptures formed along the faults and related secondary faults during the Borrego Mountain earthquake in 1968. (B) The Chainat Ridge uplift formed along the predominantly left-lateral Mae Ping fault zone in Thailand. The area of the uplift is marked by a number of north-south ridges exposing Paleozoic and Mesozoic rocks. Dark areas represent Tertiary basins (from Smith et al., 2007; reprinted with permission from The Geological Society).

will be connected by an oblique or transverse jog at an early stage, followed by the development of a structure.

Mann et al. (1983) and Mann (2007) suggested that pull-apart basins initiate along releasing bends in strike-slip faults, where the sense of slip is oblique to the trend of the segment. They further suggested that with progressive slip, the shapes of the pull-apart basins change from a spindle shape through a lazy Z or S shape to a rhomboid shape. Our experiments suggest that although the aspect ratios of the basins are controlled by the amount of extension, the shapes are also dependent on the relative positions of the strike-slip fault terminations. Oblique (45°) bends result in spindle shapes with a gentle curvature of normal faults into the strike-slip faults, whereas transverse or oblique overlapping (135°) bends or offsets result in more S or rhomboid shapes. In addition, the presence of preexisting bends or the early development of the bends in the basement fault result in narrower and deeper pull-apart basins with fewer basin-bounding faults, whereas the distribution of deformation along an offset results in a wider and deeper basin marked by a large number of smaller faults.

For restraining bends and offsets, Mann (2007) proposed that the structures evolve from gentle to sharp shapes with progressive deformation. Our experimental models show that the geometries of the structures are more dependent on the geometry of the connecting basement faults (oblique 45° , transverse, or oblique overlapping 135°), and that these geometries also control the orientations of the major uplift. Oblique (45°) bends result in more elliptical or spindle-shaped structures, whereas transverse or oblique overlapping (135°) bends result in rhomboidal or rectangular geometries. The angle between the axis of the structure and the bounding strike-slip fault segments increases progressively from approaching to transverse to overlapping offsets. A small amount of rotation of the structures commonly occurs with progressive deformation.

The nature of transfer of fault slip between the strike faults and the dip-slip faults in the area of the offset or bend controls the nature of the structures. The original models of sharp bends by Crowell (1974) involve strike-slip faults that have constant

slip until they terminate against cross faults, with an abrupt transformation from strike-slip to dip-slip faulting. Although this is one end-member possibility, our models and many natural examples suggest that a more common observation is the progressive reduction in the slip on the strike-slip faults as they approach the bends or offsets and the progressive transfer of slip to en echelon normal faults in the case of releasing bends (see also Royden, 1985) and uplifts in the case of the restraining bends. In fact, the strike-slip faults in the sedimentary cover typically break into a series of en echelon faults with very small slip in the vicinity of the bends or offsets. Typically, the bounding systems of strike-slip faults connect to only one boundary of the structure in the bend area, so that a well-connected system of faults between all four sides of the structure is very rare. The structures within the transfer zone consist primarily of normal faults with en echelon geometries in the case of releasing bends and offsets and oblique uplifts cut by reverse faults in the case of restraining bends. Secondary normal faults also form transverse or oblique to the trends of the structures.

The results of the experimental models provide details regarding the faults and related structures along restraining bends and releasing bends and offsets that can be used for interpreting both surface and subsurface structures. Most releasing and restraining bends are characterized by limited data; therefore, key relationships between the basement fault geometries, the net displacement on the faults, and the resulting geometries and orientation of folds and secondary faults can be used to improve interpretations of these structures. Characteristic differences between structural geometries of pull-apart basins and folds along restraining bends for different basement fault configurations based on the experimental models can be directly applied to subsurface structural interpretations.

Note, however, that a superficial resemblance between the geometries of natural structures and analog models is not a sufficient criterion for the assumption that a structure is related to a restraining or releasing bend. Branching and rejoining geometries of normal and reverse faults can produce similar surface patterns of fault traces as those documented for strike-slip structures, and oblique

structures bounded by such faults can be easily mistaken for strike-slip structures. The minimum criteria for interpreting the structures as strike-slip structures are that the bounding faults have a significant strike-slip component, and that the structures bounded by the faults formed at the same time as the faults and are not oblique structures cut by later strike-slip faults.

REFERENCES CITED

- Atmaoui, N., N. Kukowski, B. Stöckhert, and D. König, 2006, Initiation and development of pull-apart basins with Riedel shear mechanism: Insights from scaled clay experiments: *International Journal of Earth Sciences*, v. 95, no. 2, p. 225–238, doi:10.1007/s00531-005-0030-1.
- Aydin, A., and A. Nur, 1985, The types and role of stepovers in strike-slip tectonics, in K. T. Biddle and N. Christie-Blick, eds., *Strike-slip deformation, basin formation, and sedimentation: SEPM Special Publication 37*, p. 35–44.
- Basile, C., and J.-P. Brun, 1999, Transtensional faulting patterns ranging from pull-apart basins to transform continental margins: An experimental investigation: *Journal of Structural Geology*, v. 21, p. 23–37, doi:10.1016/S0191-8141(98)00094-7.
- Biddle, K. T., and N. Christie-Blick, eds., 1985, *Strike-slip deformation, basin formation, and sedimentation: SEPM Special Publication 37*, 386 p.
- Bose, S., and S. Mitra, 2010, Analog modeling of divergent and convergent transfer zones in listric normal fault systems: *AAPG Bulletin*, v. 94, p. 1425–1452.
- Clayton, L., 1966, Tectonic depressions along the Hope fault, a transcurrent fault in north Canterbury, New Zealand: *New Zealand Journal of Geology and Geophysics*, v. 9, no. 1–2, p. 95–104.
- Cowan, H., 1990, Late Quaternary displacements on the Hope fault at Glynn Wye, North Canterbury: *New Zealand Journal of Geology and Geophysics*, v. 33, p. 285–293.
- Crowell, J. C., 1974, Origin of late Cenozoic basins in southern California, in W. Dickinson, ed., *Tectonics and sedimentation: SEPM Special Publication 22*, p. 190–204.
- Cunningham, W. D., and P. Mann, eds., 2007, *Tectonics of strike-slip restraining and releasing bends: The Geological Society (London) Special Publication 290*, 482 p.
- Dooley, T., and K. McClay, 1997, Analog modeling of pull-apart basins: *AAPG Bulletin*, v. 81, no. 11, p. 1804–1826.
- Harding, T. P., 1985, Petroleum traps associated with wrench faults: *AAPG Bulletin*, v. 58, p. 1290–1304.
- Johnson, C. E., and D. M. Hadley, 1976, Tectonic implications of the Brawley earthquake swarm, Imperial valley, California, January 1975: *Bulletin of the Seismological Society of America*, v. 66, no. 4, p. 1133–1144.
- Kreutzer, N., 1992, Matzen field, Vienna Basin, Austria, in E. A. Beaumont and N. H. Foster, comp., *Structural traps II: AAPG Treatise of Petroleum Geology, Atlas of Oil and Gas Fields*, p. 57–98.
- Mann, P., 2007, Global catalog, classification and tectonic origins of restraining- and releasing bends on active and ancient strike-slip fault systems, in W. D. Cunningham and P. Mann, eds., *Tectonics of strike-slip restraining and releasing bends: The Geological Society (London) Special Publication 290*, p. 13–142.
- Mann, P., M. R. Hempton, D. C. Bradley, and K. Burke, 1983, Development of pull-apart basins: *Journal of Geology*, v. 91, p. 529–554, doi:10.1086/628803.
- McClay, K., and M. Bonora, 2001, Analog models of restraining stepovers in strike-slip fault Systems: *AAPG Bulletin*, v. 85, no. 2, p. 233–260.
- Morley, C. K., M. Smith, A. Carter, P. Charusiri, and S. Chantraprasert, 2007, Evolution of deformation styles at a major restraining bend, constraints from cooling histories, Mae Ping fault zone, western Thailand, in W. D. Cunningham and P. Mann, eds., in *Tectonics of strike-slip restraining and releasing bends: The Geological Society (London) Special Publication 290*, p. 325–349.
- Petrov, M., A. Talapov, T. Robertson, A. Lebedev, A. Zhilyaev and L. Polonskiy, 1998, Optical 3D digitizers: Bringing life to the virtual world: *IEEE Computer Graphics and Applications*, v. 18, p. 28–37, doi:10.1109/38.674969.
- Rahe, B., D. A. Ferrill, and A. P. Morris, 1998, Physical analog modeling of pull-apart basin evolution: *Tectonophysics*, v. 285, no. 1–2, p. 21–40, doi:10.1016/S0040-1951(97)00193-5.
- Royden, L. H., 1985, The Vienna Basin: A thin-skinned pull-apart basin, in K. T. Biddle and N. Christie-Blick, eds., *Strike-slip deformation, basin formation, sedimentation: SEPM Special Publication 37*, p. 319–338.
- Serra, S., and R. A. Nelson, 1988, Clay modeling of rift asymmetry and associated structures: *Tectonophysics*, v. 153, p. 307–312, doi:10.1016/0040-1951(88)90023-6.
- Sharp, R. V., 1967, San Jacinto fault zone in the Peninsular ranges of southern California: *Geological Society of America Bulletin*, v. 78, no. 6, p. 705–729, doi:10.1130/0016-7606(1967)78[705:SJFZIT]2.0.CO;2.
- Sharp, R. V., 1975, En echelon fault patterns of the San Jacinto fault zone: *California Division of Mines and Geology special report 18*, p. 147–152.
- Sharp, R. V., and M. M. Clark, 1972, Geologic evidence of previous faulting near the 1968 rupture on the Coyote Creek fault: *U. S. Geological Survey professional paper report P 0787*, p. 131–140.
- Smith, M., S. Chantraprasert, C. K. Morley, and I. Cartwright, 2007, Structural geometry and timing of deformation in the Chainat duplex, Thailand, in W. D. Cunningham and P. Mann, eds., *Tectonics of strike-slip restraining and releasing bends: The Geological Society (London) Special Publication 290*, p. 305–323.
- Sylvester, A. G., comp., 1984, *Wrench fault tectonics: AAPG Reprint Series 28*, 374 p.
- Tchalenko, J. S., 1970, Similarities between shear zones of different magnitudes: *Geological Society of America Bulletin*, v. 81, p. 1625–1640, doi:10.1130/0016-7606(1970)81[1625:SBSZOD]2.0.CO;2.

- Tchalenko, J. S., and N. N. Ambraseys, 1970, Structural analysis of the Dasht-e Bayaz (Iran) earthquake fractures: Geological Society of America Bulletin, v. 81, p. 41–60, doi:[10.1130/0016-7606\(1970\)81\[41:SAOTDB\]2.CO;2](https://doi.org/10.1130/0016-7606(1970)81[41:SAOTDB]2.CO;2).
- U.S. Geological Survey (USGS), 1972, The Borrego mountain earthquake of April 9, 1968: Geological Survey Professional paper report 787, 207 p.
- Wessely, G., 1988, Structure and development of the Vienna Basin in Austria, *in* L. H. Royden and F. Horváth, eds., The Pannonian Basin: A study in basin evolution: AAPG Memoir 45, p. 333–346.
- Wilcox, R. E., T. P. Harding, and D. R. Seely, 1973, Basic wrench tectonics: AAPG Bulletin, v. 57, p. 74–96.
- Wu, J. E., K. McClay, P. Whitehouse, and T. Dooley, 2009, 4D analog modeling of transtensional pull-apart basins: Marine and Petroleum Geology, v. 26, no. 8, p. 1608–1623, doi:[10.1016/j.marpetgeo.2008.06.007](https://doi.org/10.1016/j.marpetgeo.2008.06.007).